



Pyroclastic dune bedforms: macroscale structures and lateral variations. Examples from the 2006 pyroclastic currents at Tungurahua (Ecuador).

Journal:	<i>Sedimentology</i>
Manuscript ID	Draft
Manuscript Type:	Original Manuscript
Date Submitted by the Author:	n/a
Complete List of Authors:	<p>Douillet, Guilhem; Universität Bern, Institut für Geologie; Ludwig-Maximilians-Universität, Department für Geo und Umweltwissenschaften Bernard, Benjamin; Escuela Politecnica Nacional Instituto Geofisico Bouysson, Mélanie; Universite de Strasbourg Ecole et Observatoire des Sciences de la Terre, EOST Chaffaut, Quentin; Universite de Strasbourg Ecole et Observatoire des Sciences de la Terre Dingwell, Donald; Ludwig-Maximilians-Universität, Department für Geo und Umweltwissenschaften Gegg, Lukas; Universität Bern, Institut für Geologie Hoelscher, Inga; Ludwig-Maximilians-Universität, Department für Geo und Umweltwissenschaften Kueppers, Ulrich; Ludwig-Maximilians-Universität, Department für Geo und Umweltwissenschaften Mato, Célia; Universite Grenoble Alpes Ritz, Vanille; eidgenössische Technische Hochschule, Swiss Seismological Survey, Swiss Seismological Survey Schlunegger, Fritz; University of Bern, Institute of Geological Sciences Witting, Patrick; Ludwig-Maximilians-Universität, Department für Geo und Umweltwissenschaften</p>
Keywords:	Backset lamination, Dune bedforms, Pyroclastic currents, Stoss-aggradation, Tungurahua

1
2
3
4 **Pyroclastic dune bedforms: macroscale structures and lateral variations. Examples from**
5 **the 2006 pyroclastic currents at Tungurahua (Ecuador).**

6 Guilhem Amin Douillet^{1,2}, Bernard B.³, Bouyssou M.^{2,4}, Chaffaut Q.^{2,4}, Dingwell D.B.², Gegg L.^{1,2},
7 Hoelscher I.², Kueppers U.², Mato C.⁵, Ritz V.A.⁶, Schlunegger F.¹, Witting P.²

8 1: Institut für Geologie, Universität Bern, Switzerland

9 2: Earth and Environmental Sciences. Ludwig-Maximilians-Universität München, Germany

10 3: Instituto Geofísico, Escuela Politécnica Nacional, Quito, Ecuador

11 4: Ecole Et Observatoire des Sciences de la Terre, Université de Strasbourg, France

12 5: Université Joseph Fourier Grenoble, France

13 6: Swiss Seismological Service, Eidgenössische Technische Hochschule Zürich, Switzerland

14
15
16
17 **Abstract**

18 Pyroclastic currents are catastrophic flows of gas and particles triggered by explosive volcanic
19 eruptions that share much of their dynamics with particulate density currents and turbidity currents.
20 They occasionally deposit dune bedforms with peculiar lamination patterns, from what is thought to
21 represent the dilute, low concentration, and fluid-turbulence supported end member of the pyroclastic
22 currents. Here, we present a high resolution dataset of sediment plates (lacquer peels) with several
23 closely spaced lateral profiles representing sections through single pyroclastic bedforms from the
24 August 2006 eruption of Tungurahua (Ecuador).

25 Most of the sedimentary features contain backset bedding and preferential stoss-face deposition. From
26 the ripple scale (few cm) to the largest dune bedform scale (several m length), similar patterns of
27 erosive-based backset beds are evidenced. Recurrent trains of sub-vertical truncations on the stoss side
28 of bedforms reshape and steepen the bedforms. In contrast, sporadic coarse-grained lenses and
29 lensoidal lenses flatten structures by filling troughs. The coarsest (clasts up to 10 cm), least sorted and
30 massive bedforms still exhibit lineation patterns that follow the general backset architecture. Lateral
31 variations show that the bedforms vary drastically in stratal architecture within tens of centimeters,
32 and that truncations can be very local, both in flow-perpendicular and flow-parallel direction.

33 We infer that the bedforms' sedimentary patterns result from four formation mechanisms: "differential
34 draping", "slope-influenced saltation", "truncative bursts", and "granular-based events". Whereas most
35 of the literature makes a straightforward link between backset bedding and supercritical regime
36 bedforms, we demonstrate that this interpretation is not valid. Indeed, features that would be
37 diagnostic of subcritical dunes, antidunes, and cyclic steps can be found on the same horizon and in a
38 single bedform, only laterally separated by short distances (10s of cm). Rather, our data stress the
39 influence of the pulsating and highly turbulent nature of the currents that interact with pre-existing
40 morphology in a very high sedimentation environment of weak and waning currents. The role of
41 coherent flow structures such as Görtler vortices may also be significant in shaping pyroclastic
42 bedforms and influencing the dynamics of pyroclastic currents.

43 Quantification of near-bed flow velocities are made via comparison with wind tunnel experiments. We
44 estimate a pure wind velocity of 6 to 8 m.s⁻¹ could emplace the constructive bedsets, whereas the
45 truncative phases would result from bursts at 30-40 m.s⁻¹.

46 **Keywords:** Backset lamination, Dune bedforms, Pyroclastic currents, Tungurahua, stoss-aggradation

47 Running title: Pyroclastic dune bedforms from the 2006 pyroclastic currents at Tungurahua

48
49
50
51
52
53
54 **1. Introduction**

55
56
57 **1.1. Turbulent pyroclastic currents**

1
2
3 Pyroclastic currents are ground-hugging gas-pyroclast mixtures whose flow is generally driven by
4 gravity and triggered by volcanic eruptions (Dufek 2016, Sulpizio et al. 2014, Palladino 2017). A
5 range of flow processes, ranging from concentrated granular flows dominated by particle-particle
6 interactions, to fluidized mixtures and up to fully turbulent, fluid-supported currents is interpreted
7 from the study of deposits (e.g. Cole and Scarpati 1993, Fisher 1990, Branney and Kokelaar 2002,
8 Douillet et al. 2013a, Sulpizio et al. 2014). The flow-bed boundary layer is the coupling element
9 between the flow structure and the bed morphology, being influenced by and influencing both the flow
10 and the bed (Branney and Kokelaar 1992, 2002, Dellino et al. 2004a, Douillet et al. 2013a, Breard et
11 al. 2016). The processes acting at this flow-bed boundary layer have a crucial influence on the grain
12 size distribution, the texture/fabric, and depositional patterns of the sediment. Deposits containing
13 fine-scale laminasets forming dune bedforms have been interpreted as resulting from the low-
14 concentration, turbulence-dominated, end-member of pyroclastic currents (e.g. Sparks and Walker
15 1973, Cole 1990, Druitt 1992, Dellino et al. 2004b - commented by Le Roux 2005-, Douillet et al.
16 2013b). Such "dilute pyroclastic currents" may result from air entrainment due to temperature
17 buoyancy (Andrews 2014), flow stripping at cliffs (Douillet et al. 2013a), or may be related to the
18 initial eruptive dynamics, in particular for highly explosive maar volcanoes (e.g. Waters and Fisher
19 1971, Jordan et al. 2013). They are envisioned as behaving as a particular type of particulate density
20 currents, i.e. a flow with gravity as driving force, and where the agent of excess momentum is the
21 particles that will subsequently be the sediment (Simpson 1982). As such, dilute pyroclastic currents
22 are likely to be related to subaqueous turbidity currents, and a comparison of their dynamics and
23 sedimentary signature is therefore highly relevant (Branney and Kokelaar 1992, Kneller and Buckee
24 2000). A smooth transition between the granular and turbulent end-member is often modeled and
25 expected in nature (Breard et al. 2016, Burgisser and Bergantz 2002)
26
27
28
29

30 **1.2. The stoss-aggrading nature of pyroclastic bedforms**

31 Dune bedforms emplaced by pyroclastic currents are notorious for their stoss-aggrading nature
32 producing a variety of backset laminations (e.g. Schmincke et al. 1973, Cole 1991, Douillet et al.
33 2013b and references therein). Early authors have suggested that these characteristics could link to the
34 interpretation as supercritical bedforms (Fisher and Waters 1969, 1970; Waters and Fisher 1971,
35 Crowe and Fisher 1973, Mattson and Alvarez 1973, Schmincke et al. 1973). Subsequently, this stoss-
36 aggrading characteristic of the deposits has largely been taken as a straightforward argument for
37 parental supercritical flows without further debate (Fisher 1977, Yokoyama and Tokunaga 1978,
38 Wohletz and Sheridan 1979, Walker et al. 1981, Fisher et al. 1983, Suthren 1985, Sohn and Chough
39 1989, Charland and Lajoie 1989, Gianneti and Luongo 1994, Brand and White 2007, Gençlioğlu-
40 Kuşçu et al. 2007, Kelfoun et al. 2009, Brand et al. 2009, Brand and Clarke 2009, 2012). Supercritical
41 flows are defined as flows where the ratio of energy stored as kinetic energy is higher than the
42 (gravity) potential energy (and thus the dimensionless Froude number expressing this ratio is above 1,
43 e.g. Kennedy, 1963, Cartigny et al. 2011, 2014, Douillet 2015 - Chapter 2). Although supercritical
44 flows are mostly known for their upstream aggrading (backset bedding) and upper plane beds
45 signature, they can also produce laminations that aggrade downstream (e.g. Spinewine et al. 2009).
46 The direct link between backset laminations and supercritical bedforms has been questioned in the
47 pyroclastic context (e.g. Branney and Kokelaar 2002, Douillet et al. 2013b), as well as for turbidites
48 (e.g. Kubo and Nakajima 2002) and alternative interpretations have been suggested. In particular, the
49 differential draping of a fallout load in a weak current was suggested to explain the processes of
50 "regressive climbing dunes" for pyroclastic bedforms (Douillet et al. 2013b), following a similar
51 interpretation for turbidity currents (Ponce and Carmona 2011). Recently, Vellinga et al. (2018)
52 showed that for experimental turbidity currents, preferential stoss-aggradation occurs downstream of a
53 hydraulic jump, in the subcritical regions dominated by slow, vertically-expanding current.
54
55
56
57
58
59
60

The role of topography

The possibility of stoss-aggradation being forced by the inherited bed topography was put forward for turbidity currents (Nakajima and Satoh 2001, Kubo and Nakajima 2002). In the pyroclastic context, it was suggested that the shape of a bedform alone could force saltating particles to deposit preferentially on stoss-faces in a feedback effect (Douillet et al. 2014). Indeed, the saltation threshold (the minimum shear required from a current to put particles in saltation) was measured for pyroclastic particles at various bed-slopes and found to be 50% higher on stoss- vs. lee-faces (Douillet et al. 2014). The role of bed-slope has been further emphasized in the type of pyroclastic bedform produced, with evidences that dune bedforms are more likely to develop when the flow climbs up a ridge (Breard et al. 2015), that stoss-deposition is more frequent when flows climbed up-ridge than flowing down (Druitt 1992) and that giant regressive bedforms resulted from a dual bypass upstream and downstream from a depositional zone of backset beds (Brown and Branney 2004). Pyroclastic bedforms continuing their growth over several pulses or flows (e.g. Walker 1984, Cole 1991, Sulpizio et al. 2007), the interaction of the subsequent flow with the pre-existing topography can have a dominant role in sedimentation. Apart from Druitt (1992), no studies have yet addressed lateral variations within single pyroclastic bedforms, or the retro-controls of a developing bedform on its subsequent growth.

1.3. Erosional structures from turbulent pyroclastic currents

Since the recognition of the primary nature of pyroclastic dune bedforms, most documented outcrops included steep truncations of their stoss faces, generally called "chute-and-pools" and interpreted as representing the signature of hydraulic jumps in some basal layer of the flow (e.g. Schmincke et al. 1973, Gençalioglu-Kuşcu et al. 2007; Brand et al 2009). Recently, most characteristics of such stoss-side truncations, in particular their abrupt and steep termination, could be reproduced using experimental short-lived air bursts unrelated to a jump in flow regime (Douillet et al. 2017).

Under water, scours caused by wall jets have been the focus of extensive work in the engineering context (e.g. Balachandar and Reddy 2013). Interestingly, Dumas et al. (2005) noted that experimental bedforms created under combined flows had a "boxy profile" when stoss faces were steepened by intense local scouring.

Besides these truncated bedforms, erosional, longitudinal U-shaped channels formed during the flow of pyroclastic currents have intrigued volcanologists for decades. Richards (1959) documented large-scale, parallel furrows that covered the upper flanks of Barcena volcano (Mexico) briefly after the 1952 eruption. Those furrows terminated abruptly at change of slope, and large boulders were sometimes present at their upstream initiation. Similar features were reported by Kieffer and Sturtevant (1988) from the 1980 Mt. St. Helens eruption (Washington, USA). They were present in zones of flow reattachment downstream sheltered regions and were attributed to scouring by longitudinal vortices resulting from flow instabilities induced by topography. Fisher (1977) also documented U-shaped (and V-shaped) channels in stratified pyroclastic deposits, interpreted as erosion from "base surges". He suggested that a flow front would develop a "cleft and lobe pattern", with "lobes being individual turbulent cells that splay outward from the source". Thus most interpretations involve coherent structures related to a flow's turbulence.

Here, we document the sedimentary information found in pyroclastic bedforms at an unprecedented fine scale and through a survey of closely-spaced lateral transects. We show that single bedforms drastically vary in their aggrading nature, and suggest three processes of stoss-deposition unrelated to supercritical flows, which enable estimations of nearbed velocities of the parental currents.

2. The Tungurahua set of sediment plates

2.1. Context of the deposits of the 2006 eruption of Tungurahua

1
2
3 The dataset presented here was created from the unconsolidated deposits of the pyroclastic currents
4 triggered during the 17 August 2006 explosive eruption of Tungurahua volcano (Ecuador). These
5 pyroclastic currents deposited two end member sedimentary facies as a consequence of their
6 interaction with the ravines on the steep flanks of the volcano. The valley-bottom facies is dominated
7 by coarse grained, (up to metric size boulders), unsorted, massive layers (1-5 m thick, Kelfoun et al.
8 2009, Douillet et al. 2013a, Hall et al. 2013). The marginal facies occurs outside curves of valleys, on
9 shoulders and overbanks, and forms individual patches of a few 100s of meters in extent consisting of
10 fields of meter-size dune bedforms (Douillet et al. 2013b). This marginal facies is dominantly
11 composed of ash organized in cross-laminated bedsets. The marginal facies patches were interpreted
12 as resulting from locally-created, dilute and turbulent currents, when the main flow bodies would pass
13 a cliff and incorporate large amounts of air (Douillet et al. 2013a.).

14
15 These dune bedform fields represent a globally unique opportunity, as they can be investigated both in
16 terms of surficial shape, extent and internal patterns. A downstream decrease in their dimensions
17 (Douillet et al. 2013a) and evolution of outer shape has been recognized (Douillet et al. 2013b). Four
18 types of shapes were defined (Fig 1), and a spatial transition was documented from "elongate" (in
19 proximal zones), "transverse" (at the onset of deposition zones), sinusoidal and "lunate" (intermediate
20 in individual deposition zones), to "2D" bedforms (in the most distal zones of spreading). This
21 organization is very similar to that observed in the behavior of experimental turbidity currents
22 (Spinewine et al. 2009).

26 **2.2. The sediment plate dataset**

27 The dataset consists of ca. 50 m² of outcrops from the 2006 deposits. The outcrop sections were
28 hardened in their primary arrangement by impregnating the surface with epoxy, creating
29 sediment plates, a type of thick lacquer peels (see Douillet et al. in press. for the method). The
30 difference in uptake as a function of the grain size distribution for each lamina pronounces
31 sedimentary structures in the resulting plate, so that stratification is enhanced and underlined
32 to a level of detail that would not otherwise be accessible.

33
34 Sets of plates were created for each of the four types of dune bedforms previously recognized in
35 Douillet et al. (2013b): "elongate", "transverse", "lunate" and "2D" (Fig 1). For each bedform, a
36 transect consisted of a 3 m-long outcrop cut perpendicular to the crest, from the superficial
37 stoss-base to the lee, when possible reaching the entire thickness of the 2006 deposits (1 to 2.2
38 m).

39 For the transverse and lunate bedforms, several sets parallel to each other were impregnated, in
40 order to document lateral variations within a single bedform (Fig 2, 3, 4). Further, plates
41 oriented perpendicularly to the inferred flow direction were created to infer lateral continuities.
42 Finally, one 6 m long set was created from the stoss side of the transverse bedform to the crest
43 of the next one, in order to image the connection between successive structures (Fig 3, sets T1a-
44 T1b). One set of plates was made for an "elongate" bedform, a "lunate" bedform in the Chontal
45 area (later on "Chontal" transect), and two sets in two successive "2D" bedforms.

48 **3. Sedimentary structures and facies**

49 The dune bedforms are organized in laminasets and bedsets with coherent patterns separated
50 by sharp unconformities (Fig 3, 4). The general stratal architecture is characterized by partially
51 preserved lee-side (downstream dipping) bedsets, truncated by large erosive planes. These
52 truncations are either sub-horizontal or very steep (see below) and subsequently covered by
53 sets of backset laminae (upstream dipping). No conventional ripple beds were observed. Single
54 bedforms are compound of several facies types and unconformities. Whereas the transverse and
55 lunate bedforms are largely dominated by well-laminated sets of ash-size clasts (<2 mm), two
56
57
58

1
2
3 "2D" bedforms and a second lunate ("Chontal") bedform were found to have an almost massive
4 fabric, consisting of an unsorted mixture of ash (0 to 2 mm diam.), up to blocks (>5.6 cm diam.).
5 The "elongate" bedform investigated here is transitional between these coarse- and fine-grained
6 end members. Hereafter, we describe the main stratification facies based on the observations of
7 the ash dominated bedforms (Transverse, Lunate), and describe the lateral variations between
8 parallel transects in single bedforms (Transverse, Lunate). The coarse grained features (Chontal,
9 2D1, 2D2) are inventoried and discussed below in section 5 (Fig 14-17).

11 **3.1. Stoss features**

12 **a. Steep truncation trains**

13
14 The most striking and ubiquitous features are steep truncations that cut into the body of the bedforms
15 from upstream (Fig 5). These erosive contacts are subplanar over at least one meter distance in their
16 upstream part. They evolve through a sudden break in angle to steep truncations between 35 and 90°
17 (Fig 5a, d). The downstream termination of these truncations reaches the limit of the paleo-surface
18 where the crest smoothens and vanishes into apparently concordant lee-side laminae. In several cases,
19 the lee side continuation of a truncation produces shear structures which formed contemporaneously
20 with the erosive cut (see 3.2 and Douillet et al. this issue). Interestingly, these structures repeat in
21 nearby patches (Fig 5a, 7d-e). Subsequent truncations generally cut through the filling above the
22 former one (stacking upstream from each other). Truncations within a patch have relatively similar
23 dimensions but tend to become even steeper.

24 **b. Steep backsets lineations**

25
26
27 The holes that formed in response to the steep truncation events are always subsequently filled with a
28 "steep backset lineation" facies (Fig 5). The material forming the infill can either 1) have a similar
29 grain-size distribution as the undercut laminae, 2) be richer in coarser clasts (Fig 5c), 3) be depleted in
30 fines or 4) be coarser as well as fines-depleted together. The texture of the filling ranges from a
31 massive fabrics with clast-alignment patterns, to "lineated" or laminated. We use lineation here to
32 stress that some coherent sets of outlines are present, but they cannot be confidently interpreted as
33 depositional "laminae", as they may also correspond to secondary truncations within a massive
34 mixture. All of these stratigraphic indicators (truncation line, fabrics, lineations, laminations) render a
35 coherent infill plane that spans angles from 90° to <30°, adopting the morphology of the cutting, and
36 smoothing it over deposition of successive beds.

37
38 The basal (upstream) termination of these pseudo-strata are downlaps that approach the base of
39 truncations tangentially, whereas toplaps either organize as converging bundles, evolve into
40 concordant pure-aggradational crests (see 3.2.a), or form splay and fade structures. The resulting sets
41 have roughly the shape of very steep sigmoids. The steep backset lineations evolve progressively away
42 (upstream) from the erosion lines into smoother lenses or become re-incised by a subsequent
43 truncation.

44 **c. Erosive-based backsets**

45
46
47 The combination of steep truncations covered with steep backset lineations are always found together,
48 and form what is defined as "erosive-based backsets" (Fig 5a-d). Those correspond to what is often
49 described or interpreted as so-called "chute-and-pools" (see e.g. Schmincke et al. 1973, Gençalioglu-
50 Kuşcu et al. 2007, Brand and Clarke 2009).

51
52 Interestingly, the erosive-based backsets are visible at multiple scales with invariant morphology, and
53 span over two orders of magnitude with trough-to-crest heights ranging from less than 5 cm (Fig 5c) to
54 >1 m (Fig 5a). In occasions, the structural scale is correlated with the grain size distribution of the
55 subsequent infill. The smallest examples are, however, exclusively found at the base of the 2006
56 deposits, in a bedset formed of light grey silt-size ash (Fig 5c, see also Fig 10). The largest
57
58

1
2
3 documented examples in the literature (at Laacher See, Germany) reach a scale of several meters and
4 are formed by very coarse-grained lapilli (pebble-size) pumice clasts with a similar stratal architecture
5 (see Figure 8 in Douillet et al. in press, Schmincke et al. 1973). Many small-scale erosive-based
6 backsets are found as lee-side features, with a continuous transition to the backset ripple facies visible
7 on lee sides (see 3.3., Fig 7d, e).
8

9 **d. Overturning truncations**

10 The preserved laminasets immediately below truncation planes are occasionally recumbent and
11 overturned in the downflow direction on a thickness of about 1 cm and over lengths up to 15 cm (Fig
12 5e, Douillet et al. 2017). These features could be reproduced by analogue experiments using air jets
13 creating short lived bursts and will be the focus of another manuscript. They are interpreted as the
14 signature of strong basal bursts or swirls that impact the stoss-face of bedforms. This locally produces
15 an erosive airflow that is so strong that it infiltrates within the bed and coherently disturbs and
16 overturns the particle bed.
17
18

19 **e. Planar truncations**

20 Planar truncations are common and seem to be parallel to the local slope over a decameter scale.
21 They occur either as the upstream continuity of the steep truncation events, or reach a paleo-
22 surface where they vanish as apparently concordant beds. Occasionally, some planar truncations
23 cut through the whole length of a bedform (Transverse plate T1a, Elongate, 2D1, 2D2, and
24 Chontal). They are, however, not to be interpreted as a global feature linked with one particular
25 flow event at the eruption scale (Fig 6a).
26
27
28

29 **3.2. Crest features**

30 **a. Pure aggradation crests**

31 In several occurrences, the knick point of paleo-crests at a given stratigraphic level exhibits
32 continuous lamination that is preserved from the stoss to the lee side (net deposition on both
33 sides, Fig 6a, 6b). Further, the crest point is found to be shifted laterally between successive
34 laminae, and in most cases, in the upstream direction (as described for the "regressive climbing
35 dunes" in Douillet et al. 2013b). This shift of the crestlines does, however, not represent a
36 migration of the whole structures, (since the root and body of the bedforms are not translated
37 themselves) but results from preferential deposition on stoss faces.
38
39

40 **b. Prograding laminasets in regressive bedsets**

41 On the stoss-side of bedforms, individual beds seemingly massive and stoss-aggrading are in fact
42 compounds of thin, oblique, prograding laminasets of higher order –i.e. of finer scale- (Fig 6c).
43 The geometry of the containing beds is clearly stoss-aggrading (which has often been
44 interpreted as indicating supercritical flow conditions), and an upstream shift of the crest is
45 visible. However, the individual laminae inside a bed are prograding i.e. with accretion in the
46 downstream direction. Upon passing the crest of the bedform, those beds vanish on the lee side.
47
48
49

50 **3.3. Lee side features**

51 **a Planar lee laminasets**

52 Lee sides are largely dominated by steeply dipping, planar laminasets (from 10 to >25°). These
53 show strong variations in terms of lamination intensity, ranging from massive thin layers, to
54 diffuse sub-planar beds, and up to very crude and well developed laminasets. These variable
55 planar facies mainly consist of ash and the fabrics range from well-sorted to unsorted at the
56 lamina scale, involving any types of doublets from coarse to medium ash, sometimes also
57
58
59
60

1
2
3 including lapilli horizons or anecdotic outsized clasts (up to 10 cm diam., see paragraph 3.4, Fig
4 9).

6 **b. Backset ripples**

7 Numerous ripple-sized structures (albeit not necessarily genetically, but with similar
8 dimensions, ca. 10 to 30 cm length) with clear stoss aggradation and preferential upstream
9 deposition are found as part of the lee of bedforms, intercalated within the planar laminasets
10 (Fig 7a, b). They seem to be stacked on each other (in duplex), or occur with 2 or 3 periodic
11 repetitions within a synchronous bed (Fig 7d). Such backset ripples occur in close vicinity from
12 the smaller erosive-based backsets, sometimes even in train on the same horizon/isochronous
13 surface (Fig 7d, e). In few occurrences, these backset ripples can locally evolve into a
14 preferential downstream aggradation trend when aggrading in the stratigraphy, before
15 returning to a regressive trend (Fig 7c). Some of the backset ripples tend to be longer and
16 flattened (ca. 30 cm long and 5 cm thick) as well as amalgamating together, resembling small-
17 scale hummocky-cross-stratification.
18
19
20

21 **c. Overtaken shark fin structures**

22 Many horizons seem to be at the limit between erosive and concordant and occur superimposed on the
23 planar lamination trend. They include peculiar soft sediment deformation features which are
24 overturned in the flow direction and with a shark fin shape (ca. 1 cm thick; 4 cm long, Fig 8). Such
25 "shark fins" are found to be preceded upstream by a "ploughed zone" suggesting a downstream
26 migration. They were thus interpreted as shear horizons related to traction carpets on lee sides
27 (Douillet et al. 2015). More than 200 shark fins were analyzed and are the focus of the companion
28 manuscript (Douillet et al. this issue). The shark fins further occur in periodic trains on an isochrone
29 surface, and a wave mechanism was inferred to explain their formation. A linear stability analysis
30 showed that waves can develop at a shear interface without being linked with a density driven, Kelvin-
31 Helmholtz instability (Douillet et al. this issue). Shark fins often occur downstream an erosive paleo
32 crests, where the erosive line vanishes into concordant beds.
33
34
35

36 **3.4. Coarse-rich trough fillings**

37 The troughs lying between the base of a lee and stoss of the following bedform often exhibit
38 horizons containing lags of coarser material (Fig 9). Three main types of basal coarse lenses
39 were observed:
40

41 a. Superficial lags (Fig 9a): the whole surface of the 2006 bedform fields was covered by a pluri-
42 centimetric layer of centimeter diameter, light pyroclasts landed by fallout. A lens of similar
43 clasts is systematically accumulated at the base of the stoss faces. Its thickness varies around 3-
44 10 cm.
45

46 b. Outsized-clasts horizons (Fig 9b): A horizon in otherwise ash dominated bedsets contains
47 several largely outsized clasts up to >20 cm diameter. Such anecdotic horizons are laterally
48 fining into diffuse beds of centimeter-diameter clasts on their upstream continuation, and vanish
49 completely farther downstream.
50

51 c. Massive lenses and lensoidal layers (Fig 9c): a massive and relatively coarse-rich (including
52 clasts up to 5 cm) layer thickens to >10 cm on the stoss of a paleo bedform. It can be followed
53 over to the crest, but vanishes within 10s cm downstream on the lee side. In the elongate
54 bedform, the basal part of such a layer also exhibits a short dike and soft sediment deformation
55 that was interpreted as a brief intraflow injected during flow (Douillet et al. this issue).
56

57 **4. Architecture**

4.1. Basal contact

The base of the 2006 deposits is visible in the transverse and lunate sediment plates (Fig 10). When exposed, the basal unit is a thick cross-laminated bed (ca. 10 cm) of fine ash overlying coarse and weathered blocks. This zone contains numerous plant remnants, few of them carbonized, and the lamination exhibits a variety of bedding patterns. Small (few cm thick) backset ripples and erosive backsets are present. During digging out the outcrops, non-carbonized plastic ropes and farming remnants were excavated. The upper contact of this basal unit is an abrupt gradient within a few centimeters into massive to well laminated, unsorted fine to coarse-grained ash. This latter content makes the majority of the 2006 deposits up to the surface for the transverse and lunate outcrops.

4.2. Lateral variations

The counterpart of having a very detailed dataset is that correlations between transects are not evident at all, even though they come from a single bedform and are always laterally spaced by less than 1 m. Overall, a dune bedform outcrop can in no case be taken as a 2D structure, and interpretations may vary drastically within tens of centimeters. An example is suggested on the transverse (Fig 11) and lunate (Fig 12) bedforms based on the main truncations features and subsequent sedimentary facies.

a. Transverse

The transverse set consists of four parallel transects (T1-T4, Fig 11) and a perpendicular cross-profile (CP, Fig 12) linking the T3 and T4 plates in the crest area. The base of the 2006 eruption is visible in all transects but for T2.

Transect T1 is 2*3 m long (T1a & T1b) and extends to the downstream following dune crest. T1a is largely compound of downstream dipping beds lying over the basal contact of the 2006 deposits. These beds are, however, the theater for numerous trains of backset ripples and erosive-based backsets. Some shark fin structures are found on relatively isochrone beds on the lee side. The lower part of T1b presents the character of an aggrading low angle bedform, which is subsequently truncated, with the final structure developing downstream the paleo-bedform. An outsized clast horizon is present in the trough between both bedforms in the lower third infill part of the 2006 deposits. The stoss side of both successive crests consists of a large scale erosive backset zone terminating as unconformable topsets at the surface. Both of these stoss erosive backsets are not synchronous, and the genesis of the downstream bedform (T1b) predated the final shaping of the upstream one (T1a). A long planar truncation that cuts through the upper part of the whole T1a bedform is lost into conformable beds over the lower lee side.

Transect T2 contrasts in its structural patterns with those of T1. Whereas the base is not exposed, the planar truncation can still be recognized. From T2 on to the following profiles, several series of steep truncations are visible, and may have been confounded as a single truncation in T1. The four stoss-truncations identified in T2 are steepening the bedform, and are followed by episodes of stoss deposition and crest aggradation.

Transect T3 marks the onset of subvertical truncation trains. It is the steepest part of the bedform, and up to 7 trains of steep subvertical truncations followed by stoss aggrading beds are preserved. They can be correlated to some of the T2 truncations events through the infill content and degree of truncation.

Transect T4 is located below the crest edge of the bedform. Five distinct packages of truncation trains are exposed. The main train of backset laminae is translating in the upstream direction over more than 1.5 m.

1
2
3 A cross-profile connecting T3 and T4 was made in the crest area (Fig 12). It exhibits as much
4 variability as the flow-parallel profiles. Truncation events are sometimes recognized, and seen to
5 evolve with steep angles in the flow-perpendicular direction. They also cross cut each other,
6 which explains the complications upon the correlation of the individual profiles.
7

8 **b. Lunate**

9
10 The three lunate transects show more similarities between each other and the correlations are
11 more confidently proposed (Fig 13). Further, this bedform is located just 10 m upstream from
12 the transverse one, so that the same color-code is used, that may relate to the same flow events
13 as for the transverse bedform.

14 The first major truncation event visible in transects T2 and TN lies ca. 25 to 50 cm above the
15 basal fine-grained unit. This truncation surface is planar to downstream dipping, and overlain by
16 a coarse-rich horizon, a combination similar to the transect T1 and T2 from the transverse
17 bedform. Two additional truncative surfaces occur 20 to 40 cm higher in the stratigraphy, and
18 are planar downstream to slightly upstream dipping. The stoss side of the lunate bedform is, as
19 for the transverse one, cut by, three steep truncation planes that can be correlated through the
20 different profiles. The trough upstream from the stoss face is finally partially filled with a lens of
21 light pyroclasts similar to the final fallout covering the surface. A distinct discordance on the
22 upper part of the lee of transects T2 and TN-1 has been interpreted as a very short-throw
23 slumping event that produced a horizon with convolute and disturbed soft sediment
24 deformation features (Douillet et al. this issue).
25
26
27

28 **5. Coarse-grained bedforms**

29 **5.1. Elongate**

30 The elongate transect is transitional between the fine-grained bedforms and the coarser-grained
31 ones (Fig 14). It contains ash to lapilli clasts, organized in diffusely laminated bedsets to massive
32 layers up to 15 cm thick. Overall the bedform has a low angle structure and little in common
33 with the other ones in terms of stratal architecture. The base of the 2006 deposits could not be
34 observed in nearby rain-gullies cutting several meters down the surface. Sub-planar,
35 downstream dipping laminasets of low angle cross-laminations cut into each other in the lower
36 part. A low angle proto-bedform developed in the middle part of the plate, and consists of diffuse
37 and low angle backset beds. This structure is then covered by several massive to faintly
38 stratified layers with a grading contact. The latter layers are stacking up on the stoss of each
39 other, resulting in a regressive lensoidal structure.
40
41
42

43 **5.2. Chontal**

44 The Chontal bedform has the outer shape of a relatively flat lunate bedform, yet its internal
45 content is in no way comparable to the lunate bedform described earlier (Fig 15). It lies on the
46 shoulder of two valleys that directed pyroclastic currents and come closer together before a
47 sharp curve, so that the influence of two pyroclastic currents with diverging flow directions was
48 hypothesized (see the "Chontal" area in Douillet et al. 2013a). The base of the 2006 deposits
49 could not be reached, although a height of > 2 m was exposed.
50

51 Three main sedimentary phases can be identified:

52 In the lower part, a unit of ash-dominated bedsets (>50 cm thick) containing erosive-based
53 backsets and planar truncations is exposed. Its content is relatively coarse, with centimetric
54 clasts that are concentrated in the backsets' trough. This lower part contrasts with the rest of the
55 bedform, and its upper contact is very clear, although without clear sign of any truncation. This
56 unit might be related to the July 2006 pyroclastic currents rather than the ones from August.
57
58
59
60

1
2
3 A very coarse and unsorted unit (ca. 1.7 m thick) containing clasts from the ash size to blocks up
4 to ca. 10 cm diameter covers the lower ash bedsets. Whereas it appears as fairly massive at the
5 outcrop, the corresponding sediment plate exhibits several structures highlighted through an
6 undefined but perceived lineation trend. On the stoss side, signs of large and very steep (70-90°)
7 backset lineations are visible on the upper part, forming diffuse splay and fade structures. They
8 evolve into less steep backset lines over a thickness of ca. 1 m. On the lee side, planar lineations
9 are perceived. They are superimposed with a clear fining up gradient. This sedimentary facies is
10 referred to as "coarse-lineated" in the following (chapter 6.4.).

11 Finally, the third unit (10 to 35 cm thick) consists of a bedset that becomes diffusely laminated,
12 with a greater thickness on the stoss than on the lee side. Ash laminations are intercalated with
13 more massive and fining up layers.
14
15

16 **5.3. 2D bedforms**

17 The two 2D bedforms are located in an area on the counter-slope of the volcano flanks, past the
18 base of the edifice. The parental flows must have crossed the valley of the Chambo river, and
19 were interpreted as spreading against the local slope at the downstream limit of inundation of
20 the pyroclastic currents. The base of the deposits was not encountered with the sediment plates,
21 yet erosive rain-gullies testify a local thickness >4 meters.
22

23 The lower part of the transect is massive, unsorted, including blocks up to 15 cm diameter (Fig
24 16). It is overlain by a diffusely laminated, finer grained bedset, ca. 30 cm thick.
25

26 Both units are truncated on their stoss face by a layer with evidence for (i) the occurrence of
27 deposition on the stoss-side, (ii) backset lineations visible in the "2D1" bedform, and (iii) a locally
28 very varying nature from massive to diffuse lamination. Finally, a low angle, second truncation
29 of the stoss face is covered by another bedset of diffuse to massive beds consisting of ash to
30 lapilli clasts.
31

32 **6. Interpretation**

33 The numerous sedimentary features exposed in the dataset are unprecedented and bring a
34 range of novel questions. There are two ways to interpret their dynamics formation. In the
35 "traditional" scheme, the flow regime would dictate the sedimentation processes. Here, the
36 occurrence of stoss-side deposition would thus be interpreted as indicating supercritical or
37 transcritical antidunes and chute and pools. In this frame, relatively stable flows and the
38 oscillation of a free upper surface would be needed.
39

40 However, we do not favor this interpretation since most experimental and observational
41 evidences about pyroclastic currents point toward highly pulsating flows where no stable
42 conditions could develop. In that context, the bedforms' structural patterns can be well
43 explained by mechanisms driven by the basal topography and bed shapes that would interact
44 with flow bursts and pulses in highly turbulent flows at extreme sedimentation rates.
45
46

47 **6.1. Steepness and lateral variations: the invalidation of flow regime interpretations**

48 The transverse bedform is drastically evolving in terms of stratal architecture over the four
49 lateral profiles (Fig 11-14). If put in a flow-regime interpretation, T1 would likely be interpreted
50 as a subcritical dune, T2 as an antidune, whereas T3 and T4 would represent chute and pool
51 structures. It has been suggested that antidunes (indicating supercritical flows) would occur in
52 more proximal areas than chute and pools (indicating hydraulic/pneumatic jumps), and that
53 distal deposits would in turn be dominated by subcritical bedforms (e.g. Schmincke et al. 1973).
54 Our data proves that this can only be a very lucky coincidence, since the three types of stratal
55 architectures coexist in the same structure and on the same horizon. We consider it very
56
57
58

1
2
3 unlikely that three distinct flow regimes are recorded within this single bedform at the same
4 time.

5 Further, the extreme steepness of the beds contrasts with the experimental evidences of backset
6 bedding related to supercritical flows, which are generally at low angle and cross-cutting each
7 other (e.g. Alexander et al 2001, Cartigny et al. 2014, Vellinga et al. 2018). As already pointed
8 from their surface expression, the geometrical relationships of the bedforms' dimensions and
9 their steepness are not compatible with supercritical flows (Douillet et al. 2013b), an argument
10 further exacerbated by the internal patterns evidenced here. Finally, the occurrence of the same
11 structural patterns at different scales can unlikely be explained by a supercritical flow
12 interpretation (see 6.3).

13
14 In this context, we show that all features evidenced here can be interpreted without involving a
15 flows supercritical regime (see next chapters) and suggest that the sedimentary architecture is
16 dominated by the flow turbulence (related to the Reynold dimensionless number) rather than
17 by the flow regime (defined through the Froude dimensionless number).
18

19 20 **6.2. Narrow timescales: the role of turbulence**

21 The sub-vertical truncations and subsequent sub-vertical backset beds as fillings suggest highly
22 and fast varying phenomenon (Fig 5a). Their occurrence as subsequent repetitive trains further
23 suggests a pulsating behavior of flushing away and deposition within a narrow time window.
24 The organization of the filling as subvertical aggrading lamination could unlikely be reached
25 without very high sedimentation rates, and such bedsets must have deposited within seconds to
26 minutes within a pressing/plastering current (several tens of centimeters aggradation and re-
27 erosion). Such sharp transitions in sedimentary behavior testify the highly turbulent nature of
28 the flows with sudden evolution between extremes of erosive and highly depositional behaviors.
29 In 3D, the lateral variations are found to be abruptly evolving, with continuity of the order of less
30 than a meter and crest-perpendicular truncation angles up to $>30^\circ$ (Fig 12). This further
31 emphasizes that the transient phenomenon shaping bedforms are also very localized. In
32 addition, the truncations that likely remobilized large amounts of pre-deposited material are
33 also evolving within tens of centimeters in the downstream direction into concordant aggrading
34 planes. This indicates that processes of recycling and cannibalism of the sedimentary structures
35 over short distances dominate the dynamics.
36

37
38 Most erosional furrows and sharp scouring of bedforms in the literature, regarded
39 independently of a specific environment, have been perceived as resulting from coherent
40 turbulent cells (e.g. Richards 1959, Fisher 1977, Kieffer and Sturtevan 1988, Dumas et al. 2005).
41 Numerical simulations of turbulent structures over ripple beds have shown that coherent
42 structures identified as "Görtler vortices" could form and be a main agent of sediment
43 entrainment (e.g. Zedler et al. 2001). If occurring at the meter scale in pyroclastic currents, such
44 Görtler vortices would be very appropriate flow-structures to explain the formation of steep
45 truncation events. In subaqueous experiments, the scouring of stoss-faces described by Dumas
46 et al (2005) could be attributed to a similar effect. At high Reynold numbers, numerical
47 simulations succeed in reproducing low- and high-speed streaks that could impact the stoss
48 faces of bedforms (e.g. Cantero et al. 2008). Experimental turbidity currents also exhibit a
49 pulsating behavior with short time recurrences (Cartigny et al. 2013). Recent large-scale
50 pyroclastic current experiments further showed that mesoscale turbulence clusters would form
51 and concentrate particles outside turbulent eddies (Breard et al. 2016). We suggest that such
52 turbulent clusters inherent to pyroclastic currents would impact on the stoss face of bedforms as
53 erosive bursts, followed by highly depositional moments. These bursting eddies would be the
54
55
56
57
58
59
60

1
2
3 dominant mechanism that shape the stratal architecture of erosive backset events, in a similar
4 manner as the scouring described by Dumas et al (2005).

5 The steep truncations and backset lineations are similar to what is generally interpreted as
6 chute and pools (e.g. types I, II, IX of Schmincke et al. 1973, types d and e of Cole 1991), and our
7 revised interpretation may be applicable for all those structures.
8

9 10 **6.3 Scale invariant features: the importance of bed-morphology**

11 The erosive backset structures and backset ripple bedsets show a striking scale-invariance of
12 the patterns over 2 orders of magnitude (Fig 5, 7, 8). If a dimensional scaling could be simply
13 translated between the size of the structures to their parental flow process, then this would
14 mean that the same flow processes occur at different scales. In the unlikely interpretation based
15 on flow regime, this thus would imply that several sublayers of a stably density-stratified
16 pyroclastic current would experience the same transitions in dynamics at different scales and
17 velocities without interacting with the other sublayers. We do not favor this interpretation, and
18 if any scale-invariant flow process is to be favored, then the eddy downscale-cascading inherent
19 to turbulent flows would be much more likely (see Kolmogorov scale /enstrophy cascade rate,
20 e.g. Vallis 2006).
21

22 Our interpretation is that the formation of steep backsets and backset ripples is dictated by the
23 local topography and the sole consequence of high sedimentation rates. Indeed, if sedimentation
24 is high enough that any bed irregularity would trigger the formation of backset beds as a flow
25 reaction, scale is not involved and the same patterns would be obtained at any size, as observed
26 in the data.
27
28

29 **6.4. Coarse bedforms: the transitional limit between granular and turbulent flows**

30 **a. Coarse lineated facies: locally turbulent flows**

31 The high imaging power of the impregnation method enabled to identify subtle
32 lamination patterns even in the coarsest and most unsorted bedforms (e.g. Chontal &
33 2D outcrops). The coarse content and bad sorting would suggest a parental granular flow
34 behavior. However, the faint occurrence of backset and aggrading crest lineations point toward
35 traction-transport, likely related to mechanisms of support locally driven by the fluid's
36 turbulence. These bedforms may thus represent the long hypothesized transition between the
37 "dilute" (turbulent) and "concentrated" (granular) end members of pyroclastic currents (e.g.
38 Burgisser and Bergantz 2002). This strengthens our previous interpretation that the flows
39 responsible for the marginal overbank deposits locally became turbulent as a result of air
40 entrainment upon passing upstream cliffs (Douillet et al. 2013a). The closest processes that
41 might explain this coarse-lineated sedimentary facies are found in the dam break analogue
42 experiments conducted by Rowley et al (2014), where fluidized flows deposited backset,
43 lineated beds. Leclair and Arnott (2005) showed that turbidity currents with up to 36% particle
44 concentration in the bedload could deposit as laminated beds, and this ratio is suggested as an
45 order of concentration here. The fining-up, grading trends may represent a local decrease in
46 flow competence or energy but any link to the eruption dynamics is refrained.
47

48 The existence of the coarse-lineated facies further reconciliates the observation that zones
49 where the 2006 currents were interpreted as weak occurred concurrently with broken tree logs,
50 10s cm in diameter. The tilting and breaking of the logs can be imputed to the locally turbulent
51 coarse flows rather than the turbulent currents dominated by ash and weak deposition.
52
53
54

55 **b. Coarse lags: topographic pools**

56
57
58
59
60

1
2
3 The superficial lags at the base of stoss faces, formed by clasts similar to the final fallout event
4 that drape the 2006 deposits seem straightforward to interpret as a result of slight reworking
5 and winnowing of the finer-grained material by rain or wind (Fig 9a). Such features, clearly
6 interpretable here, could however be very misleading in paleo-studies where several flows are
7 stacked on top of each other.

8 Outsized clast horizons within the 2006 succession and with their isochronous, upstream and
9 downstream fading into ash dominated lamination emphasize that the grain size of the deposits
10 is not a simple function of travel distance or flow energy, but strongly influenced by local
11 topographic obstacles (Fig 9b). These horizons may represent some anecdotic pulses of
12 turbulence-enhanced granular flows, as interpreted for the coarse-laminated facies. Whereas the
13 flow capacity must be exceeded over the whole lateral continuation of the bed in order for
14 sedimentation to occur, the competence seems to have been large enough to transport large
15 clasts down to the troughs, but not make them climb up from it (see e.g. Hiscott 1994).

16 Following our previous interpretation (Douillet et al. 2013b, Douillet et al, this issue) the
17 massive, unsorted and coarse-grained nature of the lenses and lensoidal layers are considered to
18 result from parent flows with dominant particle-particle support (granular flows or bedload
19 rich) rather than fluid turbulence support (Fig 9c). The lenses vanish outside the troughs formed
20 by the upstream toe of stoss-faces and so, they flatten topography by filling the troughs. They
21 can be understood as the signature of a simple damming triggered in the pools at the toe of
22 bedforms. No particular flow conditions are required and this is understood as a pure
23 topography-triggered jamming or frictional freezing, due to the parental flows tripping against
24 the obstacle formed by bedforms (see also the caterpillar effect and intrabed flows in Douillet et
25 al. this issue).

30 **6.5. Four-fold formation mechanisms**

31 All together, the outcrops from Tungurahua enable to construct a depositional scheme for
32 pyroclastic bedforms compound of four formational bricks (Fig 17).

35 **a. Differential draping fallout**

36 The purely aggrading crests resemble climbing structures (ripples or dunes), apart for their
37 upstream preferential deposition (Fig 6a, 6b). Climbing structures are generally interpreted as
38 resulting from sedimentation with higher depositional rates than translational (e.g. Allen 1971,
39 Ashley et al. 1982). In proglacial settings, climbing-dune-cross-stratifications are related to high
40 rates of transfer of sands from suspension to the bed and net deposition on bedform stoss-sides
41 (Ghienne et al. 2010), a result likely transferable here. As already suggested for turbidites
42 (Ponce and Carmona 2011) and pyroclastic currents (Douillet et al. 2013b), we interpret that the
43 stoss-depositional crests result from a process of differential draping, whereby fallout-
44 dominated deposition is enhanced on stoss-faces, due to the simple combination of the bed
45 topography and trajectory of particles (Fig 17b). This requires the bedsets to be sedimented in a
46 gentle current with shear velocities below the saltation threshold, and high fallout input. The
47 fallout load would originate from upper parts of the pyroclastic currents, because of spatial
48 and/or temporal changes in sediment transport rate.

49 The median diameter (M_d) previously measured for the Tungurahua 2006 pyroclastic bedforms
50 at around $M_d=2 \Phi$ (Douillet et al. 2013a) can be used with the corresponding shear velocity
51 (u^*) at the saltation threshold measured for a flat bed in a wind tunnel (Douillet et al. 2014).
52 This would imply that purely aggrading crests were emplaced by weak currents with shear
53 velocities below $0.29 \text{ m}\cdot\text{s}^{-1}$, corresponding to nearbed velocities below $6 \text{ m}\cdot\text{s}^{-1}$ at a height of
54 10 cm above the bed for a pure wind.

b. Slope-forced saltation

The sets with prograding laminae on stoss faces that vanish as soon as they reach a crest are seen here as representing slightly higher shear velocities than for differential draping bedsets (Fig 6c). For these beds, the saltation threshold is partially reached, so that particles are transported near the bed. Whereas the saltation transport is sufficient to transport away all particles on a lee side, it has a net loss of carriage on stoss faces (Fig 17c). This is supported by wind tunnel measurements of the saltation threshold for pyroclasts at various bedslopes, where it was measured that the threshold is reached at up to 50% more shear velocity on a +25° slope than on a downstream dipping bed with a -25° slope (Douillet et al. 2014). Following the same comparison to wind tunnel measurements as before for the prograding stoss-laminasets, the shear velocities needed considering that the saltation threshold is reached on stoss-faces ($u^* \sim 0.39 \text{ m.s}^{-1}$) and surpassed on lee faces ($u^* > 0.27 \text{ m.s}^{-1}$) means that velocities of ca. 8 m.s^{-1} (for a pure wind) would be needed at 10 cm above the bed, slightly above the one for pure aggrading crests.

c. Truncative bursts

The steep truncations represent anomalies that disturb the previous weak-current sedimentary processes (Fig 5). Short lived, highly erosive basal pulses related to coherent turbulent structures at the flow-bed boundary are the best candidate to explain these beds, and they represent the high-energy moments of the pyroclastic currents (Fig 17d). These are directly followed by moments of very high deposition, yet lateral velocities must be present to ensure that subvertical lamination is plastered against those truncations. Those turbulent high velocity clusters must be advected in the downstream direction as well as close to the bed, in order to mainly impact on stoss faces, yet smaller ones seem to brush lee faces as well. In order to produce overturning at truncations as observed in the deposits, burst jets with velocities ranging from $28\text{-}40 \text{ m.s}^{-1}$ were needed in small scale experiments (Douillet et al. 2017), which is taken as a lower range value for the real deposits of Tungurahua, largely above the values for aggrading phases.

d. Granular based events

The coarse and massive lensoidal layers that punctually agreement bedforms' patterns represent the granular-flow part of the bedform-forming pyroclastic currents (Fig 9b-c, 17e). These sporadic events may be more common than their sedimentary signature, since the lenses often vanish as sedimentary bypasses, with no information on a granular-based passage. Little can be interpreted on the parent flow dynamics.

e. Four mechanisms and no equilibrium conditions

The whole variety of Tungurahua's bedforms can be reconstructed with a combination of the four formation mechanisms, and more generally, can be applied to most pyroclastic bedform deposits elsewhere. Notably, pyroclastic bedforms do not exhibit any kind of equilibrium structure (e.g. sustained progradation/translation). This is likely a result of rapidly changing conditions and the absence of any stable flow for long periods. These bedforms are a simple stack of the four depositional processes interacting with the pre-deposited structures. This disequilibrium is further supported by the systematic spatial stability of pyroclastic bedforms, at Tungurahua and elsewhere: Once a bed morphology is initiated, no migration is observed, over

1
2
3 several meters thickness of deposition and through the variety of depositional mechanisms.
4 Hence no stable conditions were reached during the flow of the parent pyroclastic current.
5

6 **6.5. Flow energy**

7 When interpreting sediments, we probably never look at the moments of the flow where it has
8 its highest energy, but only at the ones where deposition occur, likely always during vanishing
9 periods. As such, sediments are thus unlikely to reflect any high energy events. The most erosive,
10 and indirectly, energetic events, reported here, are the truncative bursts. All stoss-aggrading
11 features are interpreted here as low energy events. This is further supported by the fact that the
12 final depositional bedsets are almost always containing strong stoss-aggrading patterns. Thus
13 stoss-aggradation belongs to the waning periods of a pyroclastic current, where these vanish
14 rather than are highly energetic.
15

16 Even in an interpretation as "supercritical bedforms", the sedimentary beds should not be
17 related to high energy flows. Indeed, although many interpretations refer to supercritical flows
18 as highly energetic, this is a confusing statement. The flow regime, defined as sub- or super-
19 critical (or lower and upper flow regime resp.), corresponds to a flow state where the Froude
20 number (Fr) is $Fr < 1$ resp. $Fr > 1$. This ratio informs on the kinetic over potential energy of a flow,
21 but in no way on the amount of total or kinetic energy of the flow. In nature, supercritical flows
22 may in most cases represent waning, low energy conditions, rather than high energy events. We
23 thus consider that only the truncative events could be related to highly energetic events, if
24 looked at over the temporal sedimentation phases of a flow.
25
26
27

28 **Conclusion**

29 The dataset presented here represents, to date, the most extensive and fine scale investigation of
30 pyroclastic bedforms and their lateral variations. The sedimentary architecture of bedforms
31 largely consists of stoss-aggrading features, from backset ripples, erosive-based backset bedset
32 trains, draping crests with preferential stoss deposition, or lensoidal layers. They are punctuated
33 by important truncation events that attack the stoss-face of bedforms with angles up to the
34 vertical.
35

36 The presented structures can be explained through the combination of four formational
37 mechanisms, namely "differential draping", "stoss-influenced saltation", "truncative bursts", and
38 "granular-based pulses". All mechanisms involve high rates of sedimentation and weak currents.
39 The kinetic energy related to the constructive phases of the sedimentary history is likely very
40 low.
41
42

43 Coarse grained, unsorted and apparently massive deposits reveal to contain similar truncations
44 and backset beds as laminated bedforms. They represent the signature of granular currents that
45 have locally become turbulent in the vicinity of their deposition zone and testify the gradual
46 continuum between dense pyroclastic flows (granular based) and dilute pyroclastic currents
47 (turbulent supported).
48
49

50 The location of a pyroclastic bedform is spatially very stable. This contrasts with the extreme
51 variability in stratal architecture within a single dune. Within tens of centimeters, truncations
52 can reach angles of $>30^\circ$ in the flow-perpendicular direction, and pass from sub-vertical
53 truncations to concordant lamination in the flow-parallel direction. All together, the features
54 evidence that no equilibrium is reached, and that these dune bedforms are transient structures.
55 All features point toward very pulsating behavior, and the dominant role of turbulence and local
56
57
58
59
60

1
2
3 coherent turbulence structures in the vicinity of the bed (possibly Görtler vortices), interacting
4 with the topographic expression of the previously deposited bedform.
5

6 Whereas pyroclastic bedforms have long been interpreted as antidunes and chute and pools
7 related to Froude-supercritical flow regime, this interpretation is rejected here. The data proves
8 that the features usually taken as diagnostic for supercritical bedforms are only a result of local
9 scouring, drastically evolving within a single structure. The interpretation thus puts emphasis on
10 the combined role of pre-existing morphology, turbulence, and extreme sedimentation, hence
11 related to high Reynold numbers and sedimentation rates within unsteady, weak, and waning
12 currents. Quantitative estimates of nearby flow-velocity are made with comparison to wind
13 tunnel experiments on saltating pyroclasts. They suggest that a pure wind velocity of 6 to 8 m.s⁻¹
14 could emplace the constructive bedsets, whereas the truncative phases would result from bursts
15 at 30-40 m.s⁻¹.
16
17

18 **Acknowledgements**

19 This project is supported by the Deutsche Forschungsgemeinschaft grant DO1953/1-1 to GAD.
20 GAD acknowledges financial support by the Bavarian grant Thesis and BayLat. GAD and UK were
21 financially supported by the Deutsche Forschungsgemeinschaft grant KU2689/2-1. QC was
22 supported by the Alsacian grant "Boussole" All field expenses were covered through the support
23 of an ERC Advanced Grant to DBD (247076). GAD, CM, and UK thank the members of the
24 Instituto Geofísico for help at Tungurahua.
25
26
27
28
29
30
31
32
33
34
35
36
37
38
39
40
41
42
43
44
45
46
47
48
49
50
51
52
53
54
55
56
57
58
59
60

Figure captions:

Figure 1: Sketch of the four different bedform shapes identified at Tungurahua. A: Transverse, B: Lunate, C: Elongate, D: 2D.

Figure 2: Surface shape (A resp. B), and the trenches realized to impregnate the transects (C resp. D) for the of the transverse resp. lunate bedform.

Figure 3a and 3b: Transects within the Transverse bedform. Flow toward the center of the book. All transects are formed by 6 individual plates 50 cm broad, forming a 3 m long profile. Transect T1a and T1b connect to form a 6 m long profile.

Figure 4a and 4b: Transects within the lunate bedform. Flow toward the center of the book. All transects are formed by 6 individual plates 50 cm broad, forming a 3 m long profile.

Figure 5: Stoss-side features. A-C: Erosive-based backset trains at different scales, A: Bedform scale (Trans-T4P1-4), B: 10-cm-scale with coarser infilling backset bedset (Luna-T2P3), C: Small-scale in silt-sized ash. D: Vertical truncation with vertical and overhanging infill of backset lineations (Trans-T3P1). E: Truncation with overturned lamination (Luna-T3P2).

Figure 6: Crest features. A: Pure-aggradation crest bedset building on a stoss-erosive paleo crest and subsequently cut by planar truncation (Trans-T4P4). B: Pure-aggradation crest with upstream preferential deposition in the terminal sedimentation phase of growth (Trans-T2P3-4). C: Regressive (stoss-depositional) beds containing prograding laminasets. Note that laminaset vanish as soon as the paleo-crest is reached (Plate from a previously investigated transverse bedform presented in Douillet et al. 2015).

Figure 7: Backset ripples. A: Onset and growth of a fine-grained, small scale structure (TransT1b-P5). B: Onset and growth of coarse-grained structure into subvertical backset beds (TransT1aP3). C: Propagation of a backset ripple structure through the stratigraphy, with evolving behavior from preferential stoss- or lee-deposition (regressive and progressive, TransT3P4). The pink line follows the successive position of the crest. D: Patches of backset ripples and erosive based backset trains (Trans-T4P1). E: Trains of erosive-based backsets climbing in stratigraphy as well as following the same horizon.

Figure 8: Train of three shark fin structures interpreted as representing shear instabilities at the base of the flow (see Douillet et al. this issue).

Figure 9: Coarse-grained lags and lenses. A: Superficial lag formed of light gray pumice (Trans-T1bP3-6). B: Horizon with oversized clasts that vanish laterally into finer grained particles and eventually disappears (Trans-T1bP1-4). C: Relatively coarse and massive lens that forms on the stoss side of a paleo-crest and vanishes on the lee (Trans-T3P3-5).

Figure 10: Basal contact of the 2006 eruption (Trans-T1bP4). Note the coarse and weathered ground overlain by silt-sized ash beds containing uncarbonized orchid leaves (*Epidendrum Jamiesonis*) and fine scale erosive-based backset structures. The sequence is sharply coarsening-up.

Figure 11: A possible correlation of the Transverse transects. Truncations are highlighted with colors that relate to the same bursts on the different transects.

Figure 12: Cross profile between Trans T3 and Trans T4. A) Plate organization in the field. B) Interpreted relations in the downstream direction.C) Interpreted relations in the upstream direction.

Figure 13: A possible correlation of the Lunate transects. The color coding is based on the same events as for the transverse bedform (these two structures are separated by ca. 10 m in the field).

Figure 14: Interpreted transect of the Elongate bedform. This bedform is the most proximal, situated ca. 2 km up-valley from the transverse and lunate outcrops. For details on the massive lens and deformed beds, see Douillet et al. this issue.

1
2
3 **Figure 15:** A) Interpreted transect of the bedform from the Chontal area. B) Zoom of the zone
4 highlighted in A reveals the coarse-lineated facies and contact with lowermost unit.

5 **Figure 16:** Interpreted transects from the 2D bedforms. These are located in the most distal
6 deposits, situated ca. 500 m down-valley from the transverse and lunate bedforms.

7 **Figure 17:** Interpretative sketch of the four formational mechanisms for pyroclastic bedforms.
8 A) General sketch of a bedform, B) Differential draping, C) Stoss-forced saltation D) Erosive
9 basal bursts, E) Granular jamming.
10
11
12
13
14
15
16
17
18
19
20
21
22
23
24
25
26
27
28
29
30
31
32
33
34
35
36
37
38
39
40
41
42
43
44
45
46
47
48
49
50
51
52
53
54
55
56
57
58
59
60

Tables:

Plate Name	Location (valley)	Latitude	Longitude	Profiles	Type*	GPR**
Lunate	Achupashal	1°25'59.64"S	78°29'28.82"W	3*6	ash strat	No
Transverse	Achupashal	1°25'59.19"S	78°29'28.99"W	3*6+1*12	ash strat and block isol	Yes
Elongate	Achupashal	1°26'36.96"S	78°28'22.08"W	1*6	ash and lapilli strat.	Yes
2D-1	Achupashal	1°26'03.84"S	78°29'48.84"W	1*6	ash strat and lapilli mas	Yes
2D-2	Achupashal	1°26'03.48"S	78°29'48.48"W	1*4	ash strat and lapilli mas	Yes
Chontal	Juive Grande	1°25'49.08"S	78°27'14.40"W	1*6	lapilli mas and strat	Yes

Table 1: Summary of all bedforms investigated

*strat=stratified, mas=massive, isol=isolated

**GPR: A ground penetrating radar (GPR) survey was carried on the bedforms prior to their dissection and is the focus of a forthcoming manuscript - see Dujardin (2014) for preliminary results.

References

- Alexander, J., Bridge, J. S., Cheel, R. J., & Leclair, S. F. (2001) Bedforms and associated sedimentary structures formed under supercritical water flows over aggrading sand beds. *Sedimentology*, 48(1), 133-152
- Allen, J.R.L., (1971), A theoretical and experimental study of climbing-ripple cross- lamination, with a field application to the Uppsala Esker: *Geografiska Annaler, Series A, Physical Geography*, v. 53, p. 157–187.
- Andrews, B. J. (2014). Dispersal and air entrainment in unconfined dilute pyroclastic density currents. *Bulletin of Volcanology*, 76(9), 852.
- Ashley, G.M., Southard, J.B., Boothroyd, J.C., (1982), Deposition of climbing- ripple beds: a flume simulation: *Sedimentology*, v. 29, p. 67–79.
- Balachandar, R., & Reddy, H. P. (2013). Scour caused by wall jets. In *Sediment Transport Processes and Their Modelling Applications*.(edited by A.J. Manning) InTech.
- Brand, B. D., & Clarke, A. B. (2009). The architecture, eruptive history, and evolution of the Table Rock Complex, Oregon: From a Surtseyan to an energetic maar eruption. *Journal of Volcanology and Geothermal Research*, 180(2-4), 203-224.
- Brand, B. D., & Clarke, A. B. (2012). An unusually energetic basaltic phreatomagmatic eruption: using deposit characteristics to constrain dilute pyroclastic density current dynamics. *Journal of Volcanology and Geothermal Research*, 243, 81-90.
- Brand, B. D., & White, C. M. (2007). Origin and stratigraphy of phreatomagmatic deposits at the Pleistocene Sinker Butte volcano, western Snake River Plain, Idaho. *Journal of Volcanology and Geothermal Research*, 160(3-4), 319-339.
- Brand, B. D., Clarke, A. B., & Semken, S. (2009). Eruptive conditions and depositional processes of Narbona Pass Maar volcano, Navajo volcanic field, Navajo Nation, New Mexico (USA). *Bulletin of Volcanology*, 71(1), 49.
- Branney M.,J.,and Kokelaar B.P. 1992. A reappraisal of ignimbrite emplacement: Changes from particulate to non-particulate flow during progressive aggradation of high-grade•Ignimbrite Bull. *Volcanol.*,54,504-520
- Branney, M. J., Kokelaar, P., & Kokelaar, B. P. (2002). *Pyroclastic density currents and the sedimentation of ignimbrites*. Geological Society of London.
- Breard, E. C. P., Lube, G., Cronin, S. J., & Valentine, G. A. (2015). Transport and deposition processes of the hydrothermal blast of the 6 August 2012 Te Maari eruption, Mt. Tongariro. *Bulletin of Volcanology*, 77(11), 100.
- Breard, E. C., Lube, G., Jones, J. R., Dufek, J., Cronin, S. J., Valentine, G. A., & Moebis, A. (2016). Coupling of turbulent and non-turbulent flow regimes within pyroclastic density currents. *Nature Geoscience*, 9(10), 767.
- Brown, R. J., & Branney, M. J. (2004). Bypassing and diachronous deposition from density currents: Evidence from a giant regressive bed form in the Poris ignimbrite, Tenerife, Canary Islands. *Geology*, 32(5), 445-448.
- Burgisser A, Bergantz GW (2002) Reconciling pyroclastic flow and surge: The multiphase physics of pyroclastic density currents. *Earth Planet Sci Lett* 202: 405-418
- Bursik MI, Woods AW (2000) The effects of topography on sedimentation from particle-laden turbulent density currents. *J Sed Res* 70 : 53 - 63
- Cantero, M. I., Balachandar, S., García, M. H., & Bock, D. (2008). Turbulent structures in planar gravity currents and their influence on the flow dynamics. *Journal of Geophysical Research: Oceans*, 113(C8).

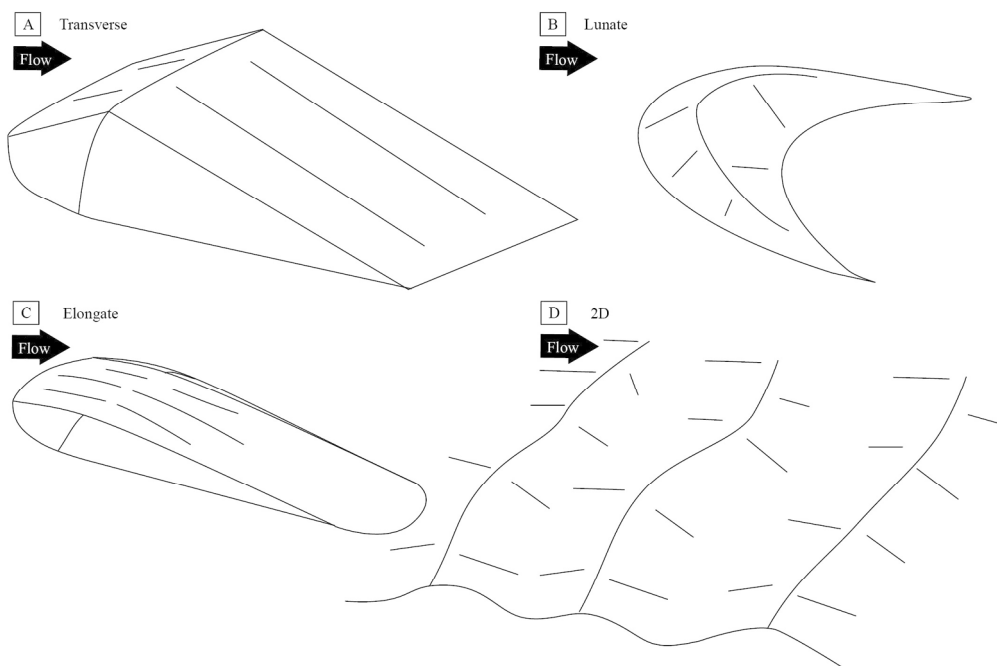
- 1
2
3 Cartigny, M. J. B., Postma, G., van den Berg, J. H. and Mastbergen, D. R. (2011) A comparative study
4 of sediment waves and cyclic steps based on geometries, internal structures and numerical modeling.
5 *Mar. Geol.*, 280, 40–56.
- 6 Cartigny, M. J., Eggenhuisen, J. T., Hansen, E. W., & Postma, G. (2013). Concentration-dependent
7 flow stratification in experimental high-density turbidity currents and their relevance to turbidite facies
8 models. *Journal of Sedimentary Research*, 83(12), 1047-1065.
- 9
10 Cartigny, M. J. B., Ventra, D., Postma, G. and van Den Berg, J. H. (2014) Morphodynamics and
11 sedimentary structures of bedforms under supercritical-flow conditions: new insights from flume
12 experiments. *Sedimentology*, 61, 712–748.
- 13 Charland, A., & Lajoie, J. (1989). Characteristics of pyroclastic deposits at the margin of Fond
14 Canonville, Martinique, and implications for the transport of the 1902 nuées ardentes of Mt. Pelée.
15 *Journal of volcanology and geothermal research*, 38(1-2), 97-112.
- 16 Cole, P. D. (1991). Migration direction of sand-wave structures in pyroclastic-surge deposits:
17 implications for depositional processes. *Geology*, 19(11), 1108-1111.
- 18
19 Cole P.D., Scarpati C. 1993. A facies interpretation of the eruption and emplacement mechanisms of
20 the upper part of the Neapolitan Yellow Tuff, Campi Flegrei, southern Italy. *Bull. Volcanol.* 55, 311-
21 326, 1993.
- 22 Crowe, B. M., & Fisher, R. V. (1973). Sedimentary structures in base-surge deposits with special
23 reference to cross-bedding, Ubehebe Craters, Death Valley, California. *Geological Society of America*
24 *Bulletin*, 84(2), 663-682.
- 25
26 Dellino, P., Isaia, R., & Veneruso, M. (2004a). Turbulent boundary layer shear flows as an
27 approximation of base surges at Campi Flegrei (Southern Italy). *Journal of Volcanology and*
28 *Geothermal Research*, 133(1-4), 211-228.
- 29
30 Dellino, P., Isaia, R., La Volpe, L., & Orsi, G. (2004b). Interaction between particles transported by
31 fallout and surge in the deposits of the Agnano–Monte Spina eruption (Campi Flegrei, Southern Italy).
32 *Journal of Volcanology and Geothermal Research*, 133(1-4), 193-210.
- 33
34 Douillet, G. A., Tsang-Hin-Sun, È., Kueppers, U., Letort, J., Pacheco, D. A., Goldstein, F., Von
35 Aulock, F., Lavallée, Y., Hanson, J. B., Bustillos, J., et al. (2013a) Sedimentology and geomorphology
36 of the deposits from the August 2006 pyroclastic density currents at Tungurahua volcano, Ecuador, *B.*
Volcanol., 75, 1–21
- 37
38 Douillet, G. A., Pacheco, D. A., Kueppers, U., Letort, J., Tsang-Hin-Sun, È., Bustillos, J., Hall, M.,
39 Ramón, P., and Dingwell, D.B. (2013b) Dune bedforms produced by dilute pyroclastic density
40 currents from the August 2006 eruption of Tungurahua volcano, Ecuador, *B. Volcanol.*, 75, 1–20,
- 41
42 Douillet, G.A., Rasmussen, K.R., Kueppers, U., Lo Castro, D., Merrison, J., Iversen, J., Dingwell,
43 D.B. (2014) Saltation threshold for pyroclasts at various bedslopes: Wind tunnel measurements. *J.*
Volc. Geotherm. Res. 278-279:14-24
- 44
45 Douillet, G.A. (2015) Flow and sedimentation from pyroclastic density currents. From large scale to
46 boundary layer processes. PhD Dissertation, October 2014, Earth and Environmental Sciences,
47 Ludwig Maximilian University, 2015
- 48
49 Douillet, G.A., Taisne, B., Tsang-Hin-Sun, E., Mueller, S.K., Kueppers, U., Dingwell, D.B. (2015)
50 Syn-eruptive, soft-sediment deformation of dilute pyroclastic density current deposits: triggers from
51 granular shear, dynamic pore pressure, ballistic impacts and shock waves. *Solid Earth Discussion*.
<http://www.solid-earth-discuss.net/6/3261/2014/sed-6-3261-2014.pdf>
- 52
53 Douillet, G.A., Bouysson, M., Gegg, L. (2017) Overturned strata in deposits of dilute pyroclastic
54 density currents, field and analogue data. IAVCEI general Assembly 2017 Portland, Oregon. Abstract
- 55
56 Douillet, G.A., Kueppers, U., Mato, C., Chaffaut, Q., Bouysson, M., Reschetizka, R., Hölscher, I.,
57 Witting, P., Hess, K.U., Cerwenka, A., Dingwell, D.B., Bernard, B. (in press) Revisiting the lacquer
58 peels method with pyroclastic deposits: Sediment plates, a precise, fine-scale imaging method and
59 powerful outreach tool. *Journal of applied Volcanology*

- 1
2
3 Douillet, G.A., Chaffaut, Q., Schlunegger, F., Kueppers, U., Dingwell, D.B. (submitted, this issue?)
4 Shark fin structures: overturned convolute and flame patterns due to waves at the shear horizon of a
5 flow-bed boundary. Examples from the deposits of the 2006 pyroclastic currents at Tungurahua
6 volcano (Ecuador). *Sedimentology*
- 7 Druitt, T.H. (1992) Emplacement of the 18 May 1980 lateral blast deposit ENE of Mount St. Helens,
8 Washington. *Bull Volcanol* 54:554–572
- 9 Dufek, J. (2016). The fluid mechanics of pyroclastic density currents. *Annual Review of Fluid*
10 *Mechanics*, 48, 459-485.
- 11 Dujardin, J. R. (2014). Imagerie géoradar (GPR) en milieu hétérogène: application aux failles actives
12 en Mongolie et aux dépôts pyroclastiques du Tungurahua (Equateur) (Doctoral dissertation, Université
13 de Strasbourg).
- 14 Dumas, S., Arnott, R. W. C., & Southard, J. B. (2005). Experiments on oscillatory-flow and
15 combined-flow bed forms: implications for interpreting parts of the shallow-marine sedimentary
16 record. *Journal of Sedimentary research*, 75(3), 501-513.
- 17 Fisher, R. V., & Waters, A. C. (1969). Bed forms in base-surge deposits: Lunar implications. *Science*,
18 165(3900), 1349-1352.
- 19 Fisher, R. V., & Waters, A. C. (1970). Base surge bed forms in maar volcanoes. *American Journal of*
20 *Science*, 268(2), 157-180.
- 21 Fisher, R.V., 1977. Erosion by volcanic base-surge density currents; U-shaped channel. *Geological*
22 *Society of America Bulletin* 88, 1287–1297.
- 23 Fisher, R. V., Schmincke, H. U., & Van Bogaard, P. (1983). Origin and emplacement of a pyroclastic
24 flow and surge unit at Laacher See, Germany. *Journal of volcanology and geothermal research*, 17(1-
25 4), 375-392.
- 26 Fisher, R. V. (1990). Transport and deposition of a pyroclastic surge across an area of high relief: the
27 18 May 1980 eruption of Mount St. Helens, Washington. *Geological Society of America Bulletin*,
28 102(8), 1038-1054.
- 29 Gençalioglu-Kuşcu, G., Atilla, C., Cas, R. A., & Kuşcu, İ. (2007). Base surge deposits, eruption
30 history, and depositional processes of a wet phreatomagmatic volcano in Central Anatolia (Cora
31 Maar). *Journal of Volcanology and Geothermal Research*, 159(1-3), 198-209.
- 32 Ghienne, J. F., Girard, F., Moreau, J., & Rubino, J. L. (2010). Late Ordovician climbing-dune cross-
33 stratification: a signature of outburst floods in proglacial outwash environments?. *Sedimentology*,
34 57(5), 1175-1198.
- 35 Giannetti, B., & Luongo, G. (1994). Trachyandesite scoria-flow and associated trachyte pyroclastic
36 flow and surge at Roccamonfina Volcano (Roman Region, Italy). *Journal of volcanology and*
37 *geothermal research*, 59(4), 313-334.
- 38 Hall, M. L., Steele, A. L., Mothes, P. A., & Ruiz, M. C. (2013). Pyroclastic density currents (PDC) of
39 the 16–17 August 2006 eruptions of Tungurahua volcano, Ecuador: Geophysical registry and
40 characteristics. *Journal of Volcanology and Geothermal Research*, 265, 78-93.
- 41 Hiscott, R. N. (1994). Loss of capacity, not competence, as the fundamental process governing
42 deposition from turbidity currents. *Journal of Sedimentary Research*, 64(2).
- 43 Jordan, S. C., Cas, R. A. F., & Hayman, P. C. (2013). The origin of a large (> 3 km) maar volcano by
44 coalescence of multiple shallow craters: Lake Purumbete maar, southeastern Australia. *Journal of*
45 *Volcanology and Geothermal Research*, 254, 5-22.
- 46 Kelfoun, K., Samaniego, P., Palacios, P., & Barba, D. (2009). Testing the suitability of frictional
47 behaviour for pyroclastic flow simulation by comparison with a well-constrained eruption at
48 Tungurahua volcano (Ecuador). *Bulletin of volcanology*, 71(9), 1057.
- 49
50
51
52
53
54
55
56
57
58
59
60

- 1
2
3 Kennedy, J. F. (1963). The mechanics of dunes and antidunes in erodible-bed channels. *Journal of*
4 *Fluid mechanics*, 16(4), 521-544.
- 5 Kieffer, S. W., & Sturtevant, B. (1988). Erosional furrows formed during the lateral blast at Mount St.
6 Helens, May 18, 1980. *Journal of Geophysical Research: Solid Earth*, 93(B12), 14793-14816.
- 7
8 Kneller, B., & Buckee, C. (2000). The structure and fluid mechanics of turbidity currents: a
9 review of some recent studies and their geological implications. *Sedimentology*, 47(s1), 62-
10 94.
- 11 Kubo, Y., & Nakajima, T. (2002). Laboratory experiments and numerical simulation of sediment-
12 wave formation by turbidity currents. *Marine Geology*, 192(1-3), 105-121.
- 13 Leclair, S. F., & Arnott, R. W. C. (2005). Parallel lamination formed by high-density turbidity
14 currents. *Journal of Sedimentary Research*, 75(1), 1-5.
- 15
16 Mattson, P. H., & Alvarez, W. (1973). Base surge deposits in Pleistocene volcanic ash near Rome.
17 *Bulletin Volcanologique*, 37(4), 553-572.
- 18 Le Roux, J. P. (2005). Comments on “Turbulent boundary layer shear flows as an approximation of
19 base surges at Campi Flegrei (Southern Italy), by Dellino et al.(2004)”. *Journal of Volcanology and*
20 *Geothermal Research*, 141(3-4), 331-332.
- 21 Nakajima, T., & Satoh, M. (2001). The formation of large mudwaves by turbidity currents on the
22 levees of the Toyama deep-sea channel, Japan Sea. *Sedimentology*, 48(2), 435-463.
- 23
24 Palladino, D. M. (2017). Simply pyroclastic currents. *Bulletin of Volcanology*, 79(7), 53.
- 25
26 Ponce, J. J., & Carmona, N. (2011). Coarse-grained sediment waves in hyperpycnal cliniform
27 systems, Miocene of the Austral foreland basin, Argentina. *Geology*, 39(8), 763-766.
- 28
29 Richards, A.F., 1959. Geology of the Islas Revillagigedo, Mexico. 1, birth and development of Volcan
30 Barcena, Isla San Benedicto (1). *Bulletin of Volcanology* 22, 73–123.
- 31 Rowley, P. J., Roche, O., Druitt, T. H., & Cas, R. (2014). Experimental study of dense pyroclastic
32 density currents using sustained, gas-fluidized granular flows. *Bulletin of Volcanology*, 76(9), 855.
- 33
34 Schmincke, H. U., Fisher, R. V., & Waters, A. C. (1973). Antidune and chute and pool structures in
35 the base surge deposits of the Laacher See area, Germany. *Sedimentology*, 20(4), 553-574.
- 36 Simpson, J. E. (1982). Gravity currents in the laboratory, atmosphere, and ocean. *Annual Review of*
37 *Fluid Mechanics*, 14(1), 213-234.
- 38
39 Sohn, Y. K., & Chough, S. K. (1989). Depositional processes of the Suwolbong tuff ring, Cheju Island
40 (Korea). *Sedimentology*, 36(5), 837-855.
- 41 Sparks, R. S. J., & Walker, G. P. L. (1973). The ground surge deposit: a third type of pyroclastic rock.
42 *Nature physical science*, 241(107), 62.
- 43
44 Spinewine, B., Sequeiros, O. E., Garcia, M. H., Beaubouef, R. T., Sun, T., Savoye, B., & Parker, G.
45 (2009). Experiments on wedge-shaped deep sea sedimentary deposits in minibasins and/or on channel
46 levees emplaced by turbidity currents. Part II. Morphodynamic evolution of the wedge and of the
47 associated bedforms. *Journal of Sedimentary Research*, 79(8), 608-628.
- 48
49 Sulpizio, R., Mele, D., Dellino, P., & La Volpe, L. (2007). Deposits and physical properties of
50 pyroclastic density currents during complex Subplinian eruptions: the AD 472 (Pollena) eruption of
51 Somma-Vesuvius, Italy. *Sedimentology*, 54(3), 607-635.
- 52
53 Sulpizio, R., Dellino, P., Doronzo, D. M., & Sarocchi, D. (2014). Pyroclastic density currents: state of
54 the art and perspectives. *Journal of Volcanology and Geothermal Research*, 283, 36-65.
- 55
56 Suthren, R. J. (1985). Facies analysis of volcanoclastic sediments: a review. Geological Society,
57 London, Special Publications, 18(1), 123-146.
- 58
59 Vallis, G.K., 2006. Atmospheric and Oceanic Fluid Dynamics—Fundamentals and Large Scale
60 Circulation. Cambridge University Press (ISBN: 978-0-521-84969-2).

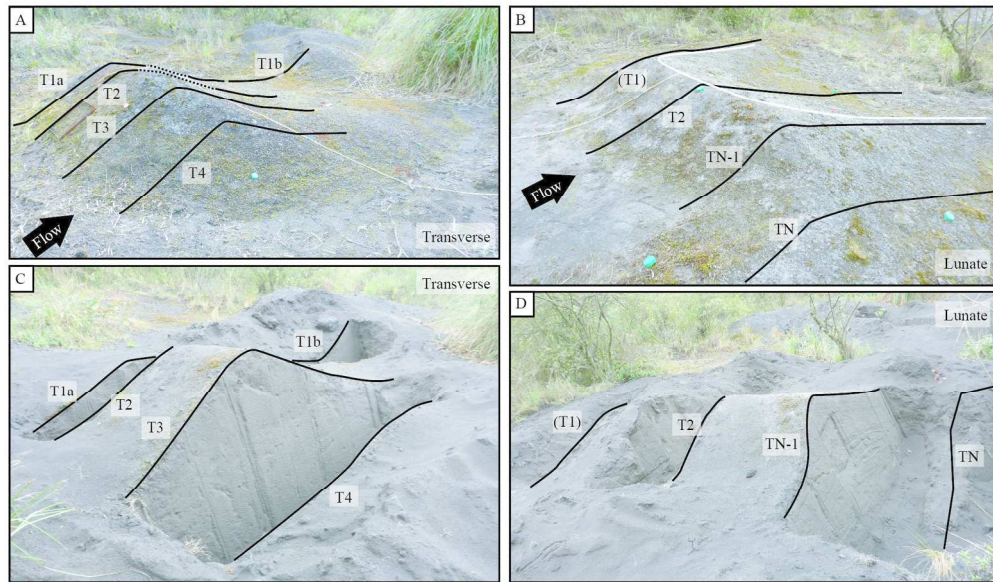
- 1
2
3 Vellinga, A. J., Cartigny, M. J., Eggenhuisen, J. T., & Hansen, E. W. (2018). Morphodynamics and
4 depositional signature of low-aggradation cyclic steps: New insights from a depth-resolved numerical
5 model. *Sedimentology*, 65(2), 540-560.
6
7 Walker, G. P. L., Wilson, C. J. N., & Froggatt, P. C. (1981). An ignimbrite veneer deposit: the trail-
8 marker of a pyroclastic flow. *Journal of Volcanology and Geothermal Research*, 9(4), 409-421.
9
10 Walker, G. P. (1984). Characteristics of dune-bedded pyroclastic surge bedsets. *Journal of*
11 *Volcanology and Geothermal Research*, 20(3-4), 281-296.
12
13 Waters, A. C., & Fisher, R. V. (1971). Base surges and their deposits: Capelinhos and Taal volcanoes.
14 *Journal of Geophysical Research*, 76(23), 5596-5614.
15
16 Wohletz, K. H., & Sheridan, M. F. (1979). A model of pyroclastic surge. *Geol Soc Am Spec Pap*, 180,
17 177-194.
18
19 Yokoyama, S., & Tokunaga, T. (1978). Base-surge deposits of Mukaiyama volcano, Nii-jima, Izu
20 Islands. *Bull Volcanol Soc Jpn*, 23, 249-262.
21
22 Zedler, E. A., & Street, R. L. (2001). Large-eddy simulation of sediment transport: currents over
23 ripples. *Journal of Hydraulic Engineering*, 127(6), 444-452.
24
25
26
27
28
29
30
31
32
33
34
35
36
37
38
39
40
41
42
43
44
45
46
47
48
49
50
51
52
53
54
55
56
57
58
59
60

1
2
3
4
5
6
7
8
9
10
11
12
13
14
15
16
17
18
19
20
21
22
23
24
25
26
27
28
29
30
31
32
33
34
35
36
37
38
39
40
41
42
43
44
45
46
47
48
49
50
51
52
53
54
55
56
57
58
59
60



Sketch of the four different bedform shapes identified at Tungurahua. A: Transverse, B: Lunate, C: Elongate, D: 2D.

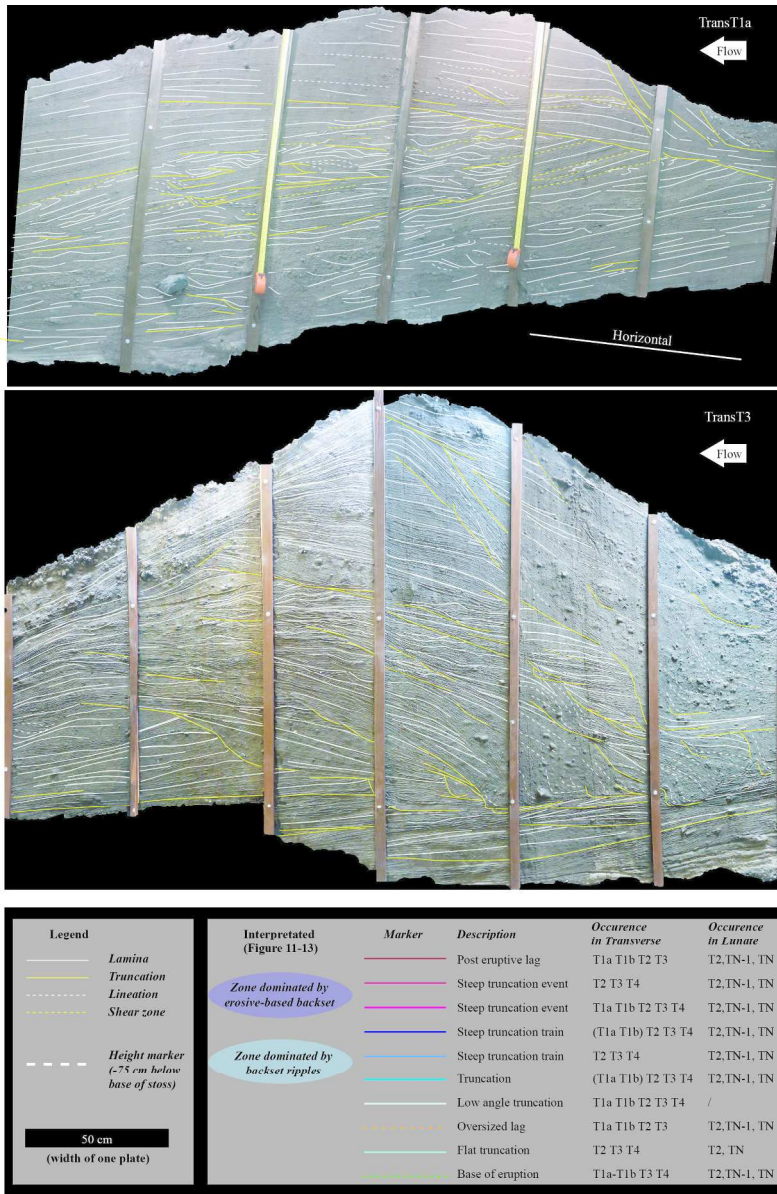
180x119mm (300 x 300 DPI)



Surface shape (A resp. B), and the trenches realized to impregnate the transects (C resp. D) for the of the transverse resp. lunate bedform.

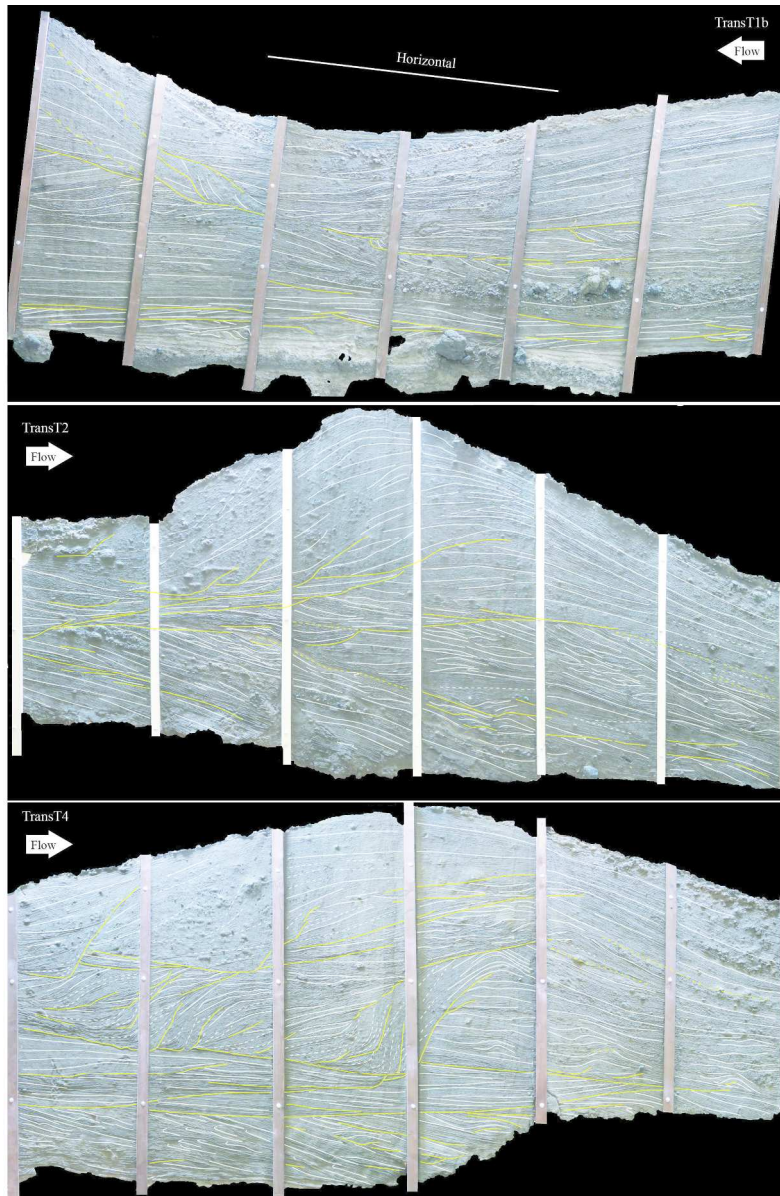
180x105mm (300 x 300 DPI)

1
2
3
4
5
6
7
8
9
10
11
12
13
14
15
16
17
18
19
20
21
22
23
24
25
26
27
28
29
30
31
32
33
34
35
36
37
38
39
40
41
42
43
44
45
46
47
48
49
50
51
52
53
54
55
56
57
58
59
60



Transects within the Transverse bedform. Flow toward the center of the book. All transects are formed by 6 individual plates 50 cm broad, forming a 3 m long profile. Transect T1a and T1b connect to form a 6 m long profile.

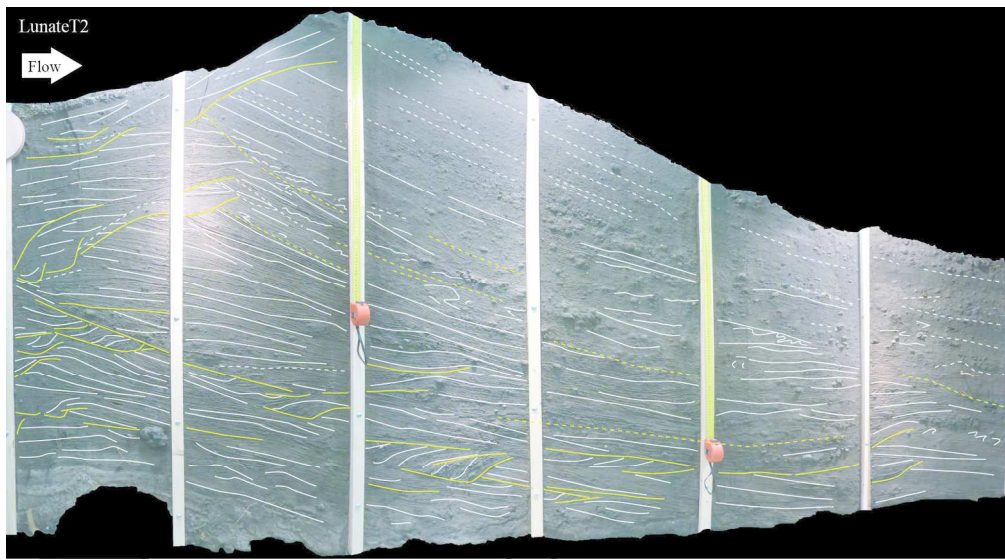
180x272mm (300 x 300 DPI)



second part of figure 3

180x272mm (300 x 300 DPI)

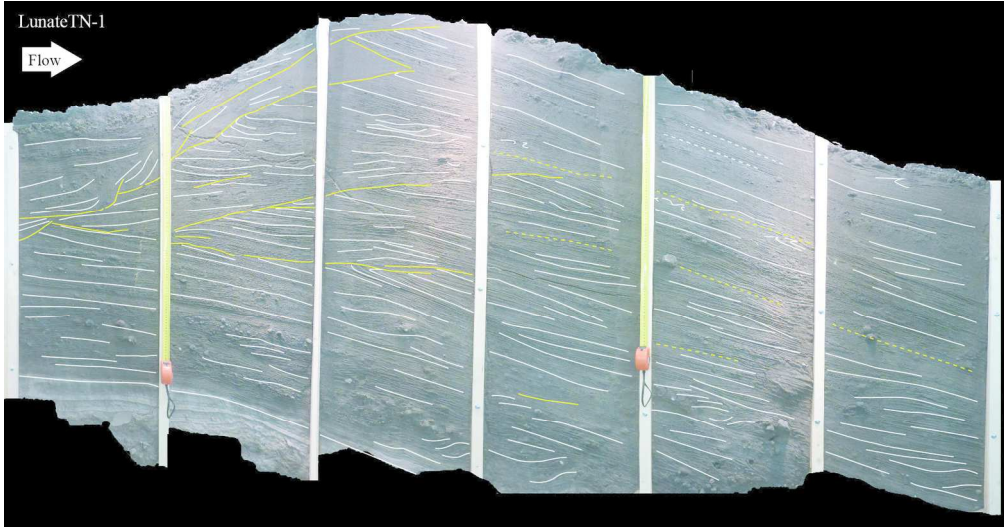
1
2
3
4
5
6
7
8
9
10
11
12
13
14
15
16
17
18
19
20
21
22
23
24
25
26
27
28
29
30
31
32
33
34
35
36
37
38
39
40
41
42
43
44
45
46
47
48
49
50
51
52
53
54
55
56
57
58
59
60



Transects within the lunate bedform. Flow toward the center of the book. All transects are formed by 6 individual plates 50 cm broad, forming a 3 m long profile.

176x97mm (300 x 300 DPI)

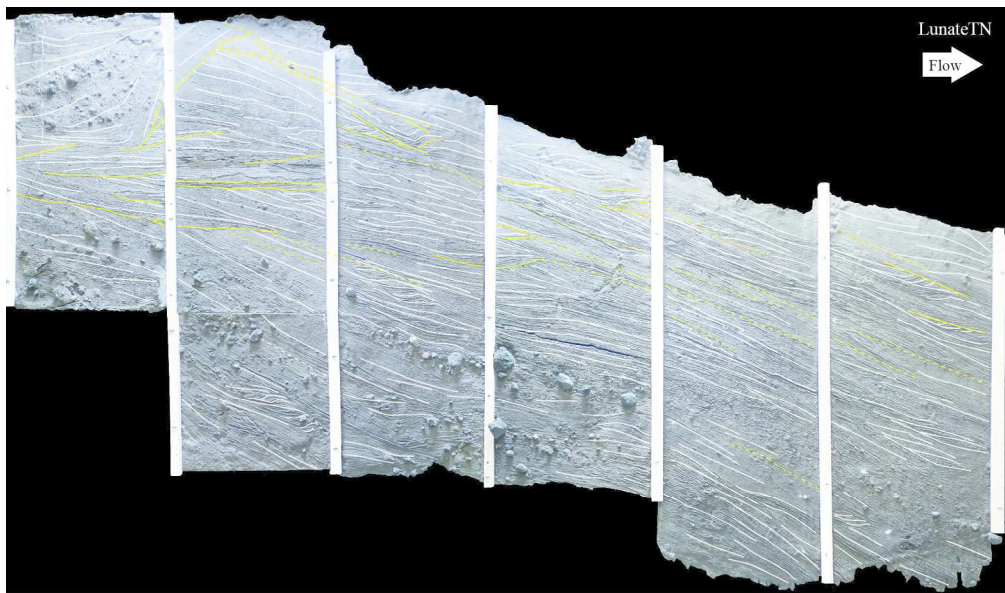
1
2
3
4
5
6
7
8
9
10
11
12
13
14
15
16
17
18
19
20
21
22
23
24
25
26
27
28
29
30
31
32
33
34
35
36
37
38
39
40
41
42
43
44
45
46
47
48
49
50
51
52
53
54
55
56
57
58
59
60



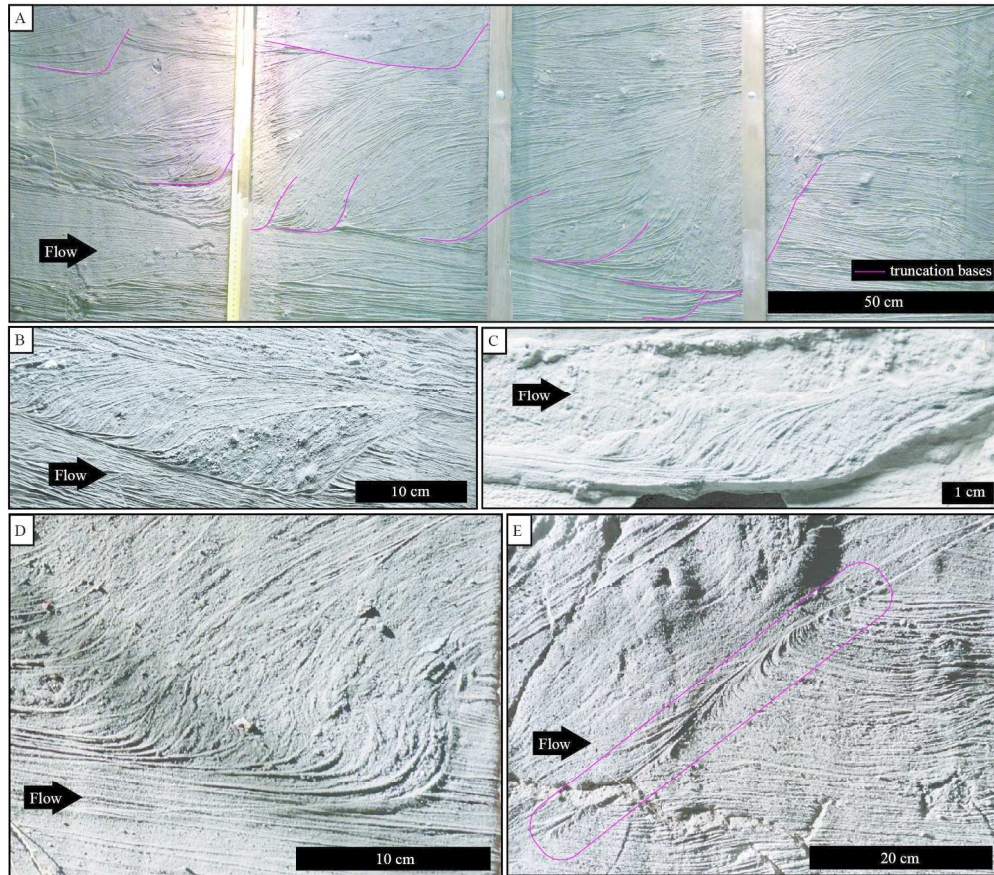
second part of lunate transects

177x93mm (300 x 300 DPI)

1
2
3
4
5
6
7
8
9
10
11
12
13
14
15
16
17
18
19
20
21
22
23
24
25
26
27
28
29
30
31
32
33
34
35
36
37
38
39
40
41
42
43
44
45
46
47
48
49
50
51
52
53
54
55
56
57
58
59
60

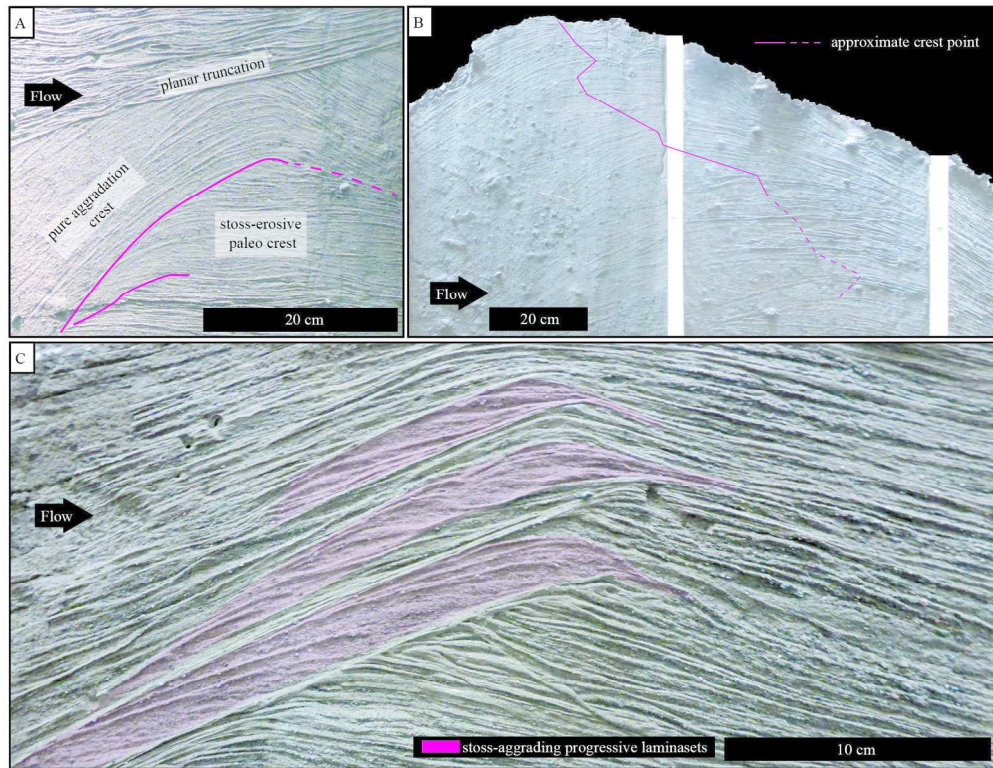


third part of lunate transects
177x104mm (300 x 300 DPI)



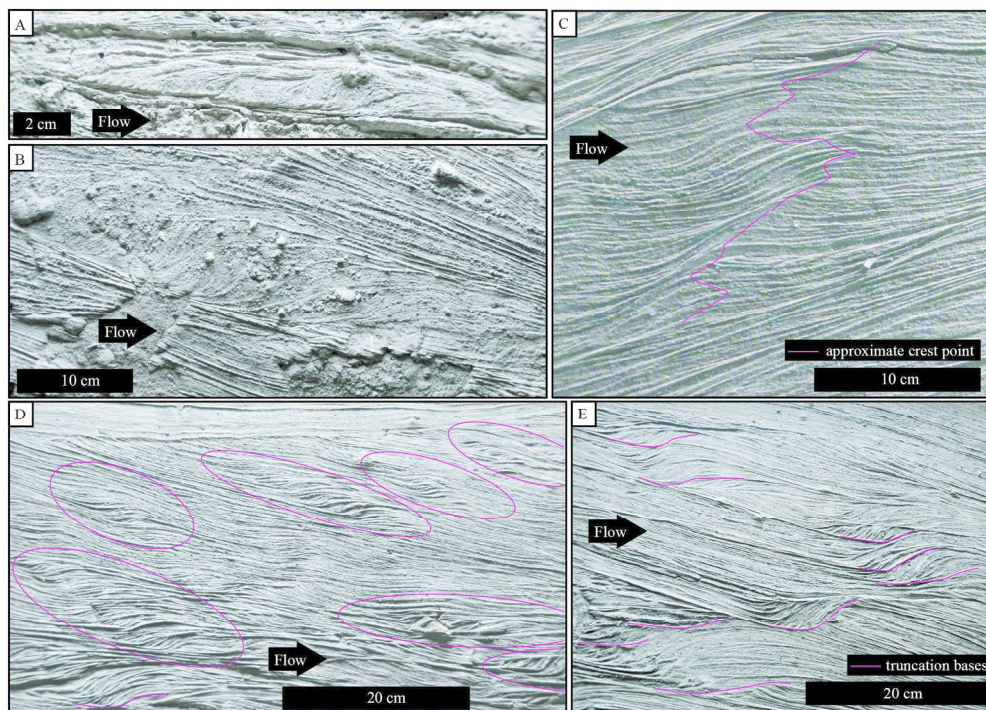
Stoss-side features. A-C: Erosive-based backset trains at different scales, A: Bedform scale (Trans-T4P1-4), B: 10-cm-scale with coarser infilling backset bedset (Luna-T2P3), C: Small-scale in silt-sized ash. D: Vertical truncation with vertical and overhanging infill of backset lineations (Trans-T3P1). E: Truncation with overturned lamination (Luna-T3P2).

180x157mm (300 x 300 DPI)



Crest features. A: Pure-aggradation crest bedset building on a stoss-erosive paleo crest and subsequently cut by planar truncation (Trans-T4P4). B: Pure-aggradation crest with upstream preferential deposition in the terminal sedimentation phase of growth (Trans-T2P3-4). C: Regressive (stoss-depositional) beds containing prograding laminasets. Note that laminasets vanish as soon as the paleo-crest is reached (Plate from a previously investigated transverse bedform presented in Douillet et al. 2015).

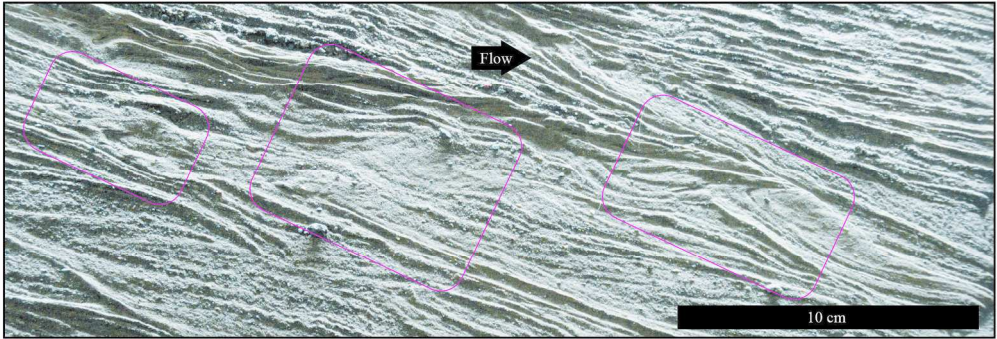
180x139mm (300 x 300 DPI)



Backset ripples. A: Onset and growth of a fine-grained, small scale structure (TransT1b-P5). B: Onset and growth of coarse-grained structure into subvertical backset beds (TransT1aP3). C: Propagation of a backset ripple structure through the stratigraphy, with evolving behavior from preferential stoss- or lee-deposition (regressive and progressive, TransT3P4). The pink line follows the successive position of the crest. D: Patches of backset ripples and erosive based backset trains (Trans-T4P1). E: Trains of erosive-based backsets climbing in stratigraphy as well as following the same horizon.

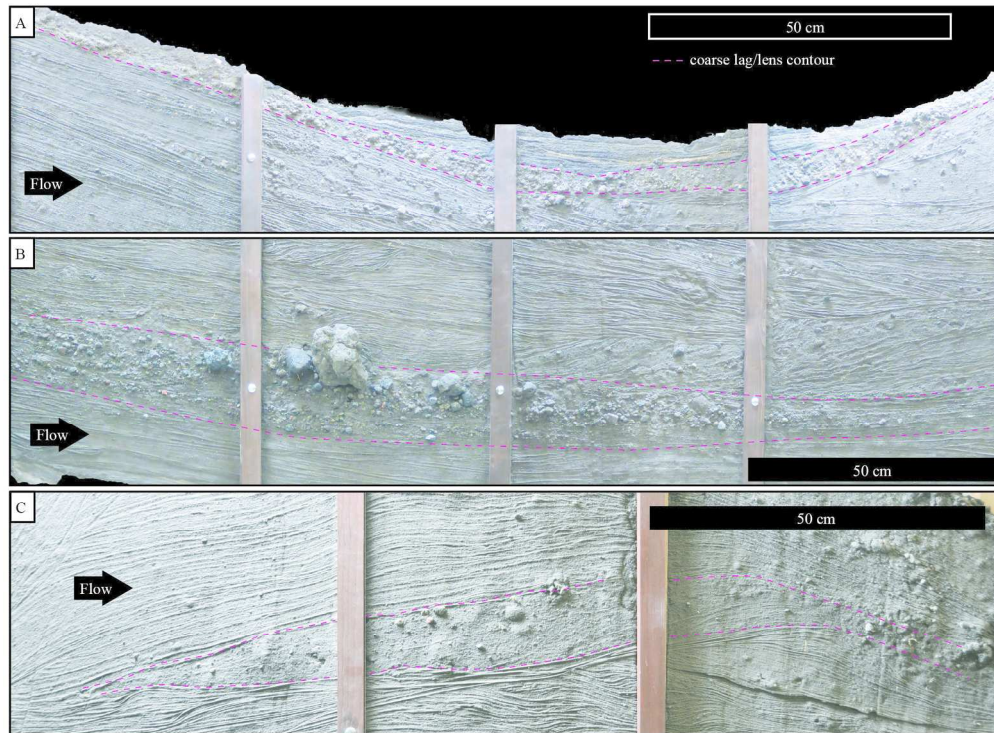
180x128mm (300 x 300 DPI)

1
2
3
4
5
6
7
8
9
10
11
12
13
14
15
16
17
18
19
20
21
22
23
24
25
26
27
28
29
30
31
32
33
34
35
36
37
38
39
40
41
42
43
44
45
46
47
48
49
50
51
52
53
54
55
56
57
58
59
60



Train of three shark fin structures interpreted as representing shear instabilities at the base of the flow (see Douillet et al. this issue).

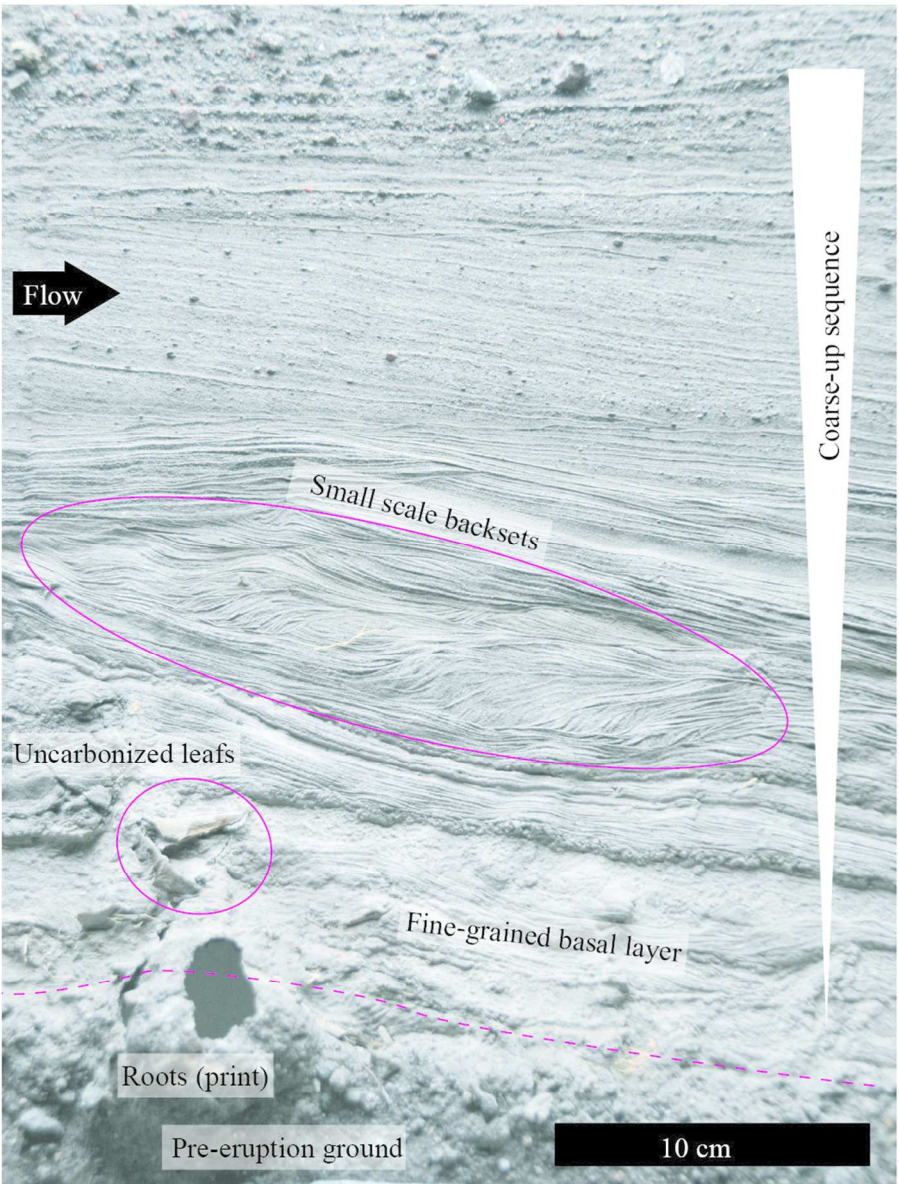
180x61mm (300 x 300 DPI)



Coarse-grained lags and lenses. A: Superficial lag formed of light gray pumice (Trans-T1bP3-6). B: Horizon with oversized clasts that vanish laterally into finer grained particles and eventually disappears (Trans-T1bP1-4). C: Relatively coarse and massive lens that forms on the stoss side of a paleo-crest and vanishes on the lee (Trans-T3P3-5).

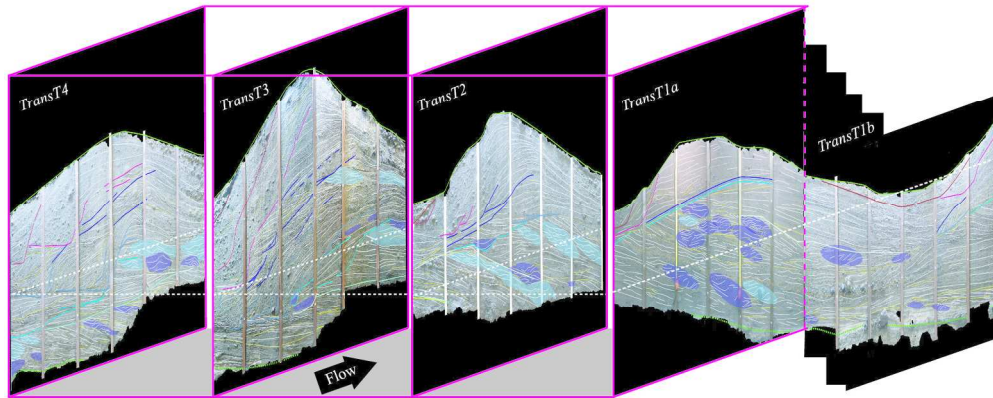
180x132mm (300 x 300 DPI)

1
2
3
4
5
6
7
8
9
10
11
12
13
14
15
16
17
18
19
20
21
22
23
24
25
26
27
28
29
30
31
32
33
34
35
36
37
38
39
40
41
42
43
44
45
46
47
48
49
50
51
52
53
54
55
56
57
58
59
60



asal contact of the 2006 eruption (Trans-T1bP4). Note the coarse and weathered ground overlain by silt-sized ash beds containing uncarbonized orchid leaves (*Epidendrum Jamiesonis*) and fine scale erosive-based backset structures. The sequence is sharply coarsening-up.

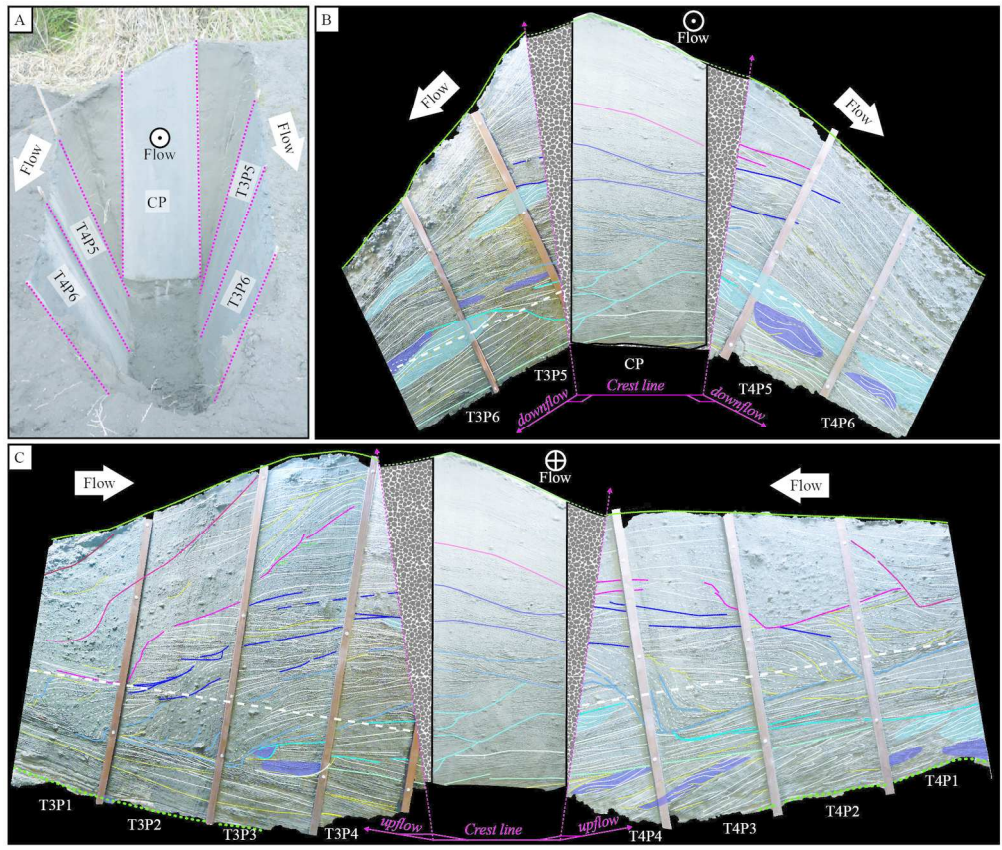
90x118mm (300 x 300 DPI)



A possible correlation of the Transverse transects. Truncations are highlighted with colors that relate to the same bursts on the different transects.

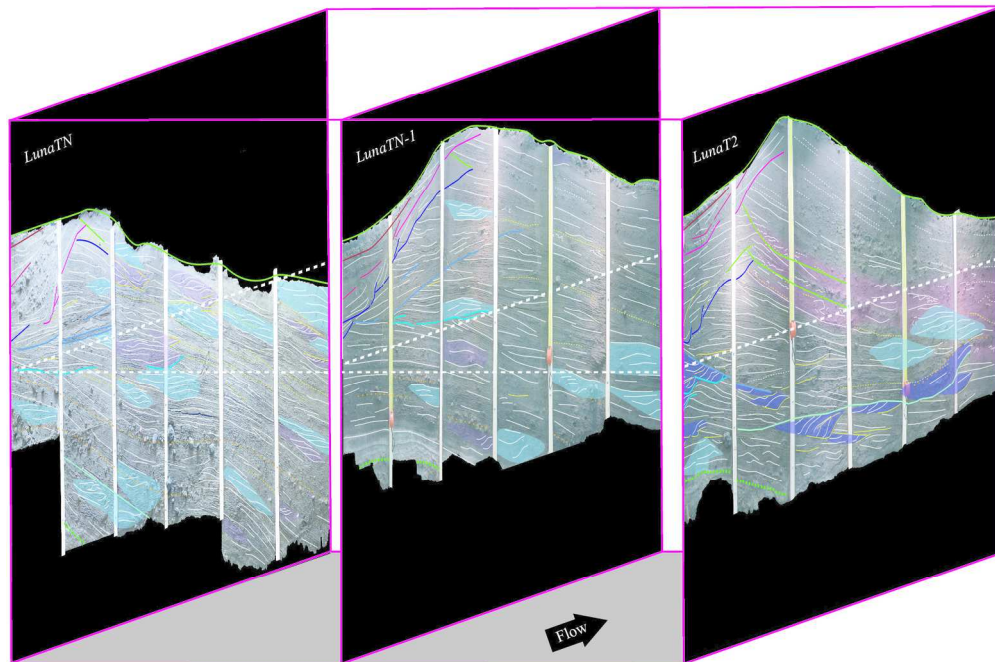
180x74mm (300 x 300 DPI)

1
2
3
4
5
6
7
8
9
10
11
12
13
14
15
16
17
18
19
20
21
22
23
24
25
26
27
28
29
30
31
32
33
34
35
36
37
38
39
40
41
42
43
44
45
46
47
48
49
50
51
52
53
54
55
56
57
58
59
60



Cross profile between Trans T3 and Trans T4. A) Plate organization in the field. B) Interpreted relations in the downstream direction. C) Interpreted relations in the upstream direction.

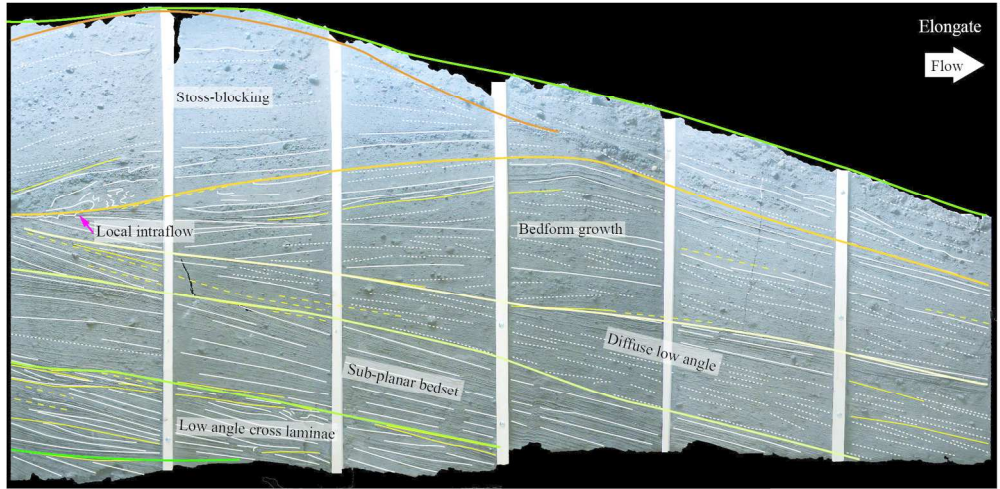
180x152mm (300 x 300 DPI)



A possible correlation of the Lunate transects. The color coding is based on the same events as for the transverse bedform (these two structures are separated by ca. 10 m in the field).

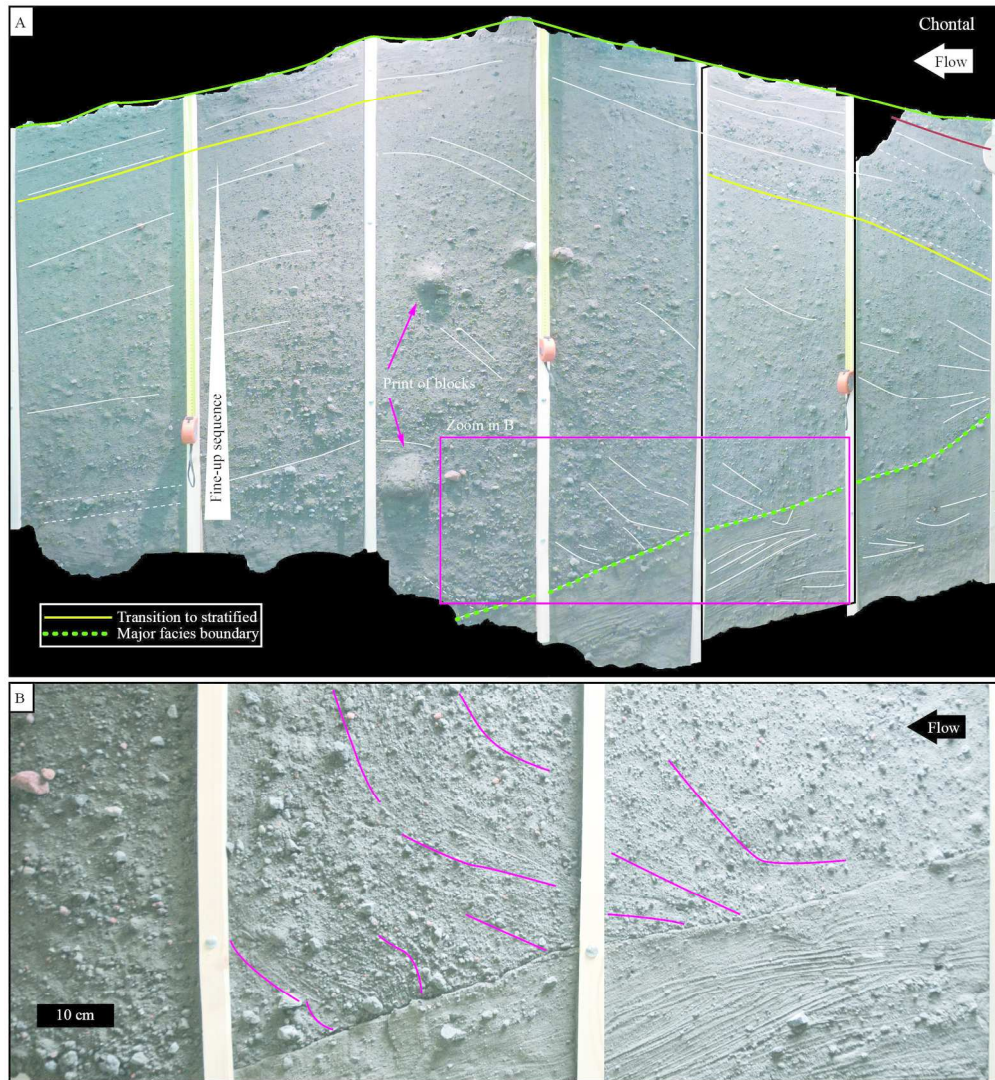
180x121mm (300 x 300 DPI)

1
2
3
4
5
6
7
8
9
10
11
12
13
14
15
16
17
18
19
20
21
22
23
24
25
26
27
28
29
30
31
32
33
34
35
36
37
38
39
40
41
42
43
44
45
46
47
48
49
50
51
52
53
54
55
56
57
58
59
60



Interpreted transect of the Elongate bedform. This bedform is the most proximal, situated ca. 2 km up-valley from the transverse and lunate outcrops. For details on the massive lens and deformed beds, see Douillet et al. this issue.

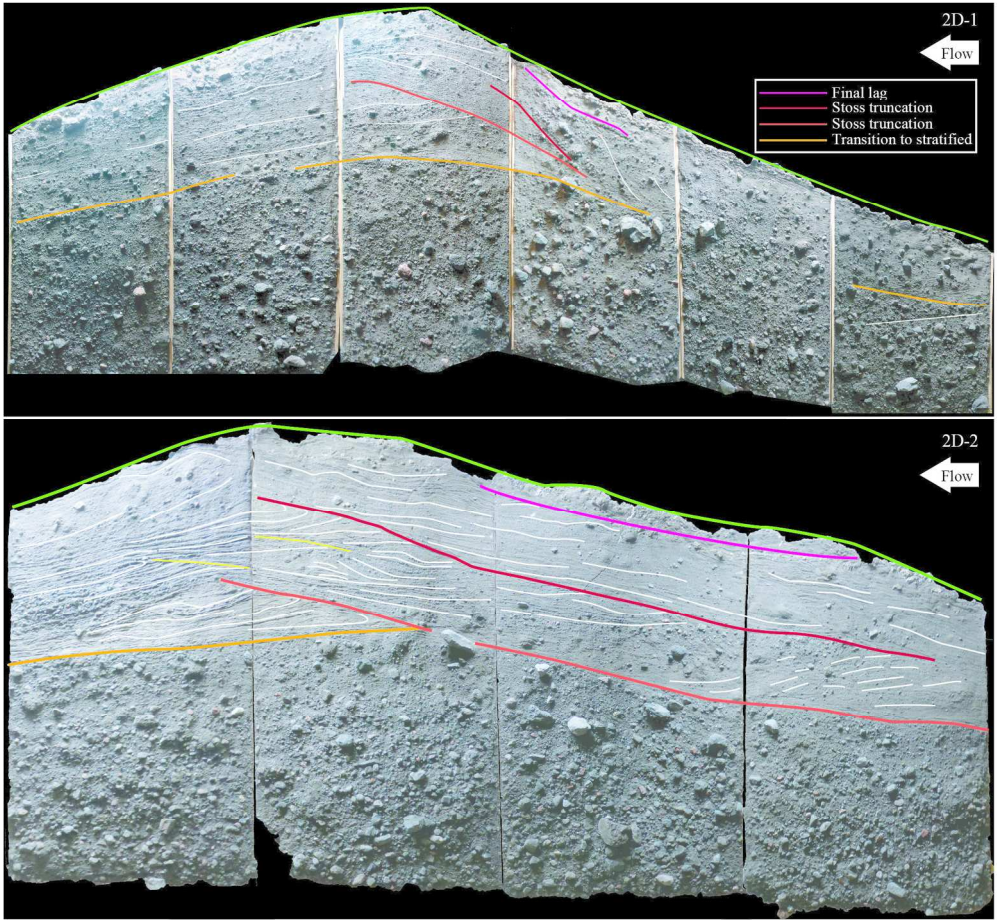
180x88mm (300 x 300 DPI)



A) Interpreted transect of the bedform from the Chontal area. B) Zoom of the zone highlighted in A reveals the coarse-lineated facies and contact with lowermost unit.

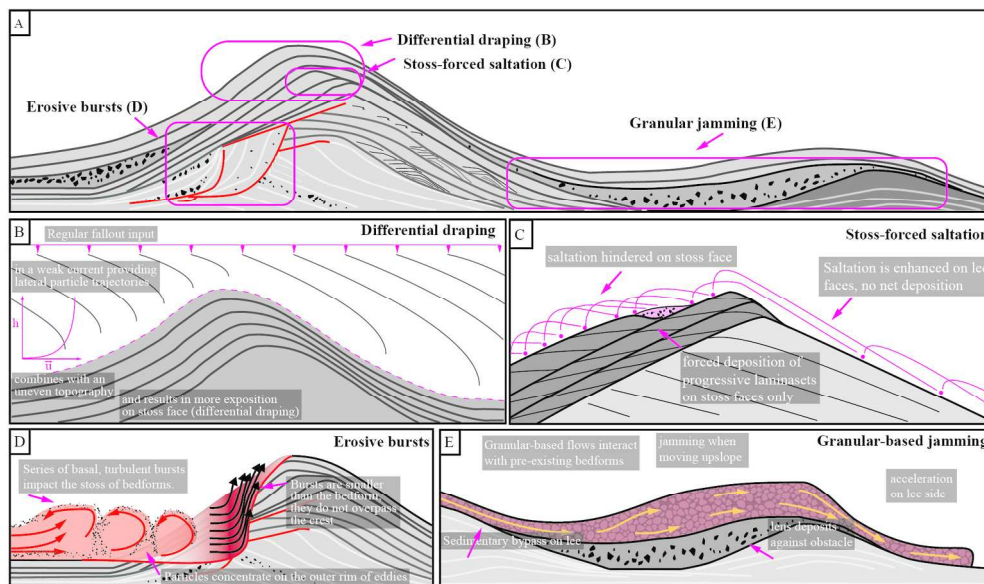
180x196mm (300 x 300 DPI)

1
2
3
4
5
6
7
8
9
10
11
12
13
14
15
16
17
18
19
20
21
22
23
24
25
26
27
28
29
30
31
32
33
34
35
36
37
38
39
40
41
42
43
44
45
46
47
48
49
50
51
52
53
54
55
56
57
58
59
60



Interpreted transects from the 2D bedforms. These are located in the most distal deposits, situated ca. 500 m down-valley from the transverse and lunate bedforms.

180x166mm (300 x 300 DPI)



Interpretative sketch of the four formational mechanisms for pyroclastic bedforms. A) General sketch of a bedform, B) Differential draping, C) Stoss-forced saltation D) Erosive basal bursts, E) Granular jamming.

180x106mm (300 x 300 DPI)